THE ASTROPHYSICAL JOURNAL, 444:647–662, 1995 May 10

THE STELLAR CONTENT OF 30 DORADUS DERIVED FROM SPATIALLY INTEGRATED ULTRAVIOLET SPECTRA: A TEST OF SPECTRAL SYNTHESIS MODELS

WILLIAM D. VACCA[1,2]
Astronomy Department, 601 Campbe Hall, University of California, Berkeley, CA 94720
CARMELLE ROBERT AND CLAUS LEITHERER
Space Telescope Science Institute, 3700 San Martin Drive, Baltimore, MD 21218; crobert, leitherer@stsci.edu
AND
PETER S. CONTI
Joint Institute for Laboratory Astrophysics, Campus Box 440, University of Colorado, Boulder, CO 80309; pconti@jila.colorado.edu
Received 1994 April 25; accepted 1994 October 26

ABSTRACT

Using the *IUE* satellite, we have obtained spatially integrated ultraviolet spectra of three areas within the giant H II region 30 Dor in the Large Magellanic Cloud. The spectra correspond to spatial regions with sizes of 20″ × 20″, 1′ × 1′, and 3′ × 3′, all of which are approximately centered on R136. We have performed a spectral synthesis analysis of the spectra of the two larger regions and compared the results with the known stellar content in these regions. The spectral synthesis models are sensitive to the ultraviolet continuum level, the P Cygni profile of the C IV λ1550 line, the absorption strength of the Si IV λ1400 line, and the emission strength of the He II λ1640 line. The intrinsic continuum levels and the profiles of these stellar wind lines provide constraints on the age and duration of the starburst episode within a region, as well as on the upper cutoff mass of the initial mass function. From our analysis we find that the present-day value of the upper cutoff mass in the 1′ × 1′ and 3′ × 3′ regions has a lower limit of $\sim 50\ M_{\odot}$, a result which is in good agreement with several other recent determinations. The age of the starburst episode must be less than ~3 Myr, also in agreement with other estimates. Comparison of the observed total numbers of O and W-R stars with those predicted from the various models favors an instantaneous burst of star formation in the regions. However, the differences between the two burst scenarios we investigated (instantaneous and continuous) are small at such a young age, and distinguishing between the two is difficult. We are now confident that these spectral synthesis models can be used to determine the stellar content of more distant star-forming regions.

Subject headings: galaxies: stellar content — H II regions — Magellanic Clouds — open clusters and associations: individual (30 Doradus) — stars: luminosity function, mass function — ultraviolet: stars

1. INTRODUCTION

The giant H II region known as 30 Dor (=N157 = LH 100 = NGC 2070), located on the eastern side of the Large Magellanic Cloud (LMC), is one of the largest star-forming regions in the Local Group. It contains a large population of OB stars and a substantial fraction of the known Wolf-Rayet (W-R) stars in the LMC (Melnick 1985; Moffat et al. 1987; Lee 1990; Lortet & Testor 1991; Walborn 1991a, b; Hill et al. 1993; Parker 1992, 1993; Malumuth & Heap 1994). The center of the region is marked by the compact stellar cluster R136, which itself contains several W-R stars and a number of hot stars (Walborn 1986; Weigelt et al. 1991; Campbell et al. 1992; Heap, Ebbets, & Malumuth 1992; De Marchi et al. 1993; Malumuth & Heap 1994). Reviews of the stellar content of 30 Dor and R136 have been given by Walborn (1984, 1986, 1991a). General reviews of the overall properties of the 30 Dor nebula have been given by Meylan (1993) and Kennicutt & Chu (1994).

Due to the substantial numbers of hot, young, massive stars, which are evidence of a recent burst of star formation within the region, 30 Dor serves as the prototype for more distant giant extragalactic H II regions and the star-forming regions in H II, W-R, and starburst galaxies. Indeed, 30 Dor is often considered the "Rosetta Stone" for the interpretation of these objects (Walborn 1991b).

As one of the few extragalactic H II regions in which individual components (stars and clumps of emitting gas) can be spatially resolved, 30 Dor provides a unique opportunity to study the detailed structure and composition of a massive star-forming/starburst region and compare the predictions of theoretical models of such regions with observations. The proximity and apparent size of the nebula have naturally led observers to study numerous small sections of the region in detail (e.g., Mathis, Chu, & Peterson 1985; Rosa & Mathis 1987). However, for a better understanding of distant H II and starburst regions whose various stellar and gaseous components cannot be resolved, a comparison of the *global* properties of the 30 Dor nebula with the known stellar content and the conditions in smaller subregions is needed. The tremendous importance of 30 Dor to distant starburst regions lies in this unique possibility of linking the global properties of the region with its small-scale structure and individual components.

We have attempted to forge this link by approaching the problem of the determination of the stellar population in 30 Dor from a "global" perspective. Using the *International Ultraviolet Explorer* (*IUE*) and a rarely employed "drift-scan"

[1] Hubble Fellow and Beatrice Watson Parrent Fellow.
[2] Present address: Institute for Astronomy, 2680 Woodlawn Drive, Honolulu, HI 96822; vacca@galileo.ifa.hawaii.edu.

method of observing, we have obtained "spatially integrated" UV spectra of three regions, with sizes of 20″ × 20″, 1′ × 1′, 3′ × 3′, centered on the core of 30 Dor. The drift-scan technique allowed us to obtain spectra which simulate what would be observed from the region if 30 Dor were located at a cosmological distance. We use the spectral synthesis routines developed by Leitherer, Robert, & Drissen (1992b) and Robert, Leitherer, & Heckman (1993) to analyze these spatially integrated UV spectra and determine the parameters of the hot star populations within the various regions. The UV wavelength regime is ideally suited for this study because several spectral features arising from the winds and photospheres of O, B, and W-R stars are found in the UV and they provide a means of estimating the hot star content. In addition, the hot stars produce a substantial UV continuum, which can also be used to determine the stellar population. The results of the models are used to place constraints on the upper cutoff mass of the initial mass function (IMF), as well as the age of the starburst episode, in the observed regions. The massive star content inferred from the observed integrated spectra is also compared with the *known* hot star population derived directly from star counts. In particular, the results of our spectral analysis are compared with the estimates of the massive stellar content of 30 Dor determined from both ground-based photometry and spectroscopy (Parker 1992, 1993; Parker & Garmany 1993) and the recent images obtained with the *Hubble Space Telescope* (*HST*) (Campbell et al. 1992; DeMarchi et al. 1993; Malumuth & Heap 1994). Thus, the spatially integrated spectra of these regions and the subsequent analyses provide critical and unprecedented tests of stellar atmosphere and spectral synthesis models and the validity of their results when applied to complex systems.

In a subsequent paper, the results derived here will be compared with those found from modeling spatially integrated optical spectra of the same regions (Vacca, Conti, & Phillips 1995). By combining multiwavelength images and spectra with the observed stellar number counts, a more complete picture of this giant extragalactic H II region should emerge. This can then be used as a foundation for the study of H II and star-forming regions in other galaxies.

The *IUE* observations and data reduction methods are discussed in § 2. The spectral synthesis models used here are described in § 3. The application of these models to the data is presented in § 4, and a discussion of the results is given in § 5. Our conclusions are summarized in § 6.

2. OBSERVATIONS AND DATA REDUCTION

The observations of 30 Dor were carried out with the *IUE* satellite during one US2 observing shift on 1991 July 3, one US1 shift on 1991 July 3–4, and one US2 shift on 1992 April 21. All observations were made through the large (nominally 10″ × 20″) aperture with the SWP camera in low-resolution mode. (The aperture is actually an oval with dimensions of approximately 9.″1 × 21.″6; Garhart 1992a.) Data were acquired using a drift-scan technique in which the satellite was pointed at an initial position and then forced to drift over ("scan") the target area at a controlled rate while the detector accumulated data. Data accumulation was temporarily interrupted when the satellite reached a predetermined position (the end of a scan). The satellite was then repositioned for the start of the next scan (which was offset in either right ascension or declination from the previous scan) and the procedure was repeated. The individual scans were always oriented in a cardinal direction, approximately perpendicular to the long axis of the aperture, and were offset from one another by ~20″. Care was taken to ensure that individual scans did not overlap one another substantially. During the 1991 July observations each scan was performed in the north-south direction; during the 1992 April observations the scans were in the east-west direction. With this technique an SWP spectral image for a spatially extended region was obtained.

We acquired data for three regions approximately centered on R136 ($\alpha_{1950} = 5^h39^m38^s.5$, $\delta_{1950} = -69°07'35''.2$). Two SWP images for a 20″ × 20″ region were acquired with one scan each, while the image for the 1′ × 1′ region was accumulated during three scans and that for the 3′ × 3′ region was obtained with 10 scans.[3] At a distance of 51.2 kpc, as given by Panagia et al. (1991), the three regions have physical sizes of ~5 pc × 5 pc (20″ × 20″), ~15 pc × 15 pc (1′ × 1′), and ~45 pc × 45 pc (3′ × 3′). Because the position angle θ_{pa} of the major axis of the large aperture was not exactly perpendicular to the scan directions for these observations, the regions are not perfectly square. The approximate locations of the three regions covered during the observations are shown in Figure 1 (Plate 15). Additional details of the observations are given in Table 1.

The four spectra corresponding to the various spatial regions were extracted from the raw SWP images using the "optimal" weighted-slit extraction algorithms (Horne 1986) implemented for *IUE* low-dispersion data reduction (Kinney, Bohlin, & Neill 1991). We refer the reader to the papers by Horne (1986) and Kinney et al. (1991) for a detailed description of the extraction algorithms. Briefly, these routines (1) determine the background level in the *IUE* SWP image and subtract it from the image, (2) fit an instrumental profile perpendicular to the dispersion axis at each wavelength, (3) identify cosmic-ray hits and "bad" data pixels using the instrumental profile and a model of the noise in an *IUE* SWP image, (4) weight the remaining data points at each wavelength according to their position in the instrumental profile and their estimated noise values, and (5) determine the flux number at

[3] Originally, nine scans were planned to cover this large region. However, due to an error in initial positioning, two of the scans over the 3′ × 3′ region partially overlapped; the overlap region is a strip ~14.″5 × 3′. An extra scan was added to partially compensate for the error. As a result, the region covered during this observation is actually 3.′1 × 3′, and R136 is located slightly to the west of the center of the region.

TABLE 1

IUE OBSERVATIONS OF 30 DOR

Image	Date	Region	t_{total} (s)	t_{eff} (s)	N_{scans}	Scan Rate (arcsec s^{-1})	Scan Direction	θ_{pa}
SWP 41991.....	1991 Jul 3	20″ × 20″	300	143	1	0.0333	N-S	88°
SWP 41995.....	1991 Jul 3	20″ × 20″	300	143	1	0.0333	N-S	89
SWP 41999.....	1991 Jul 4	3′ × 3′	19980	101	10	0.0851	N-S	89
SWP 44450.....	1992 Apr 21	1′ × 1′	2700	145	3	0.0556	E-W	19

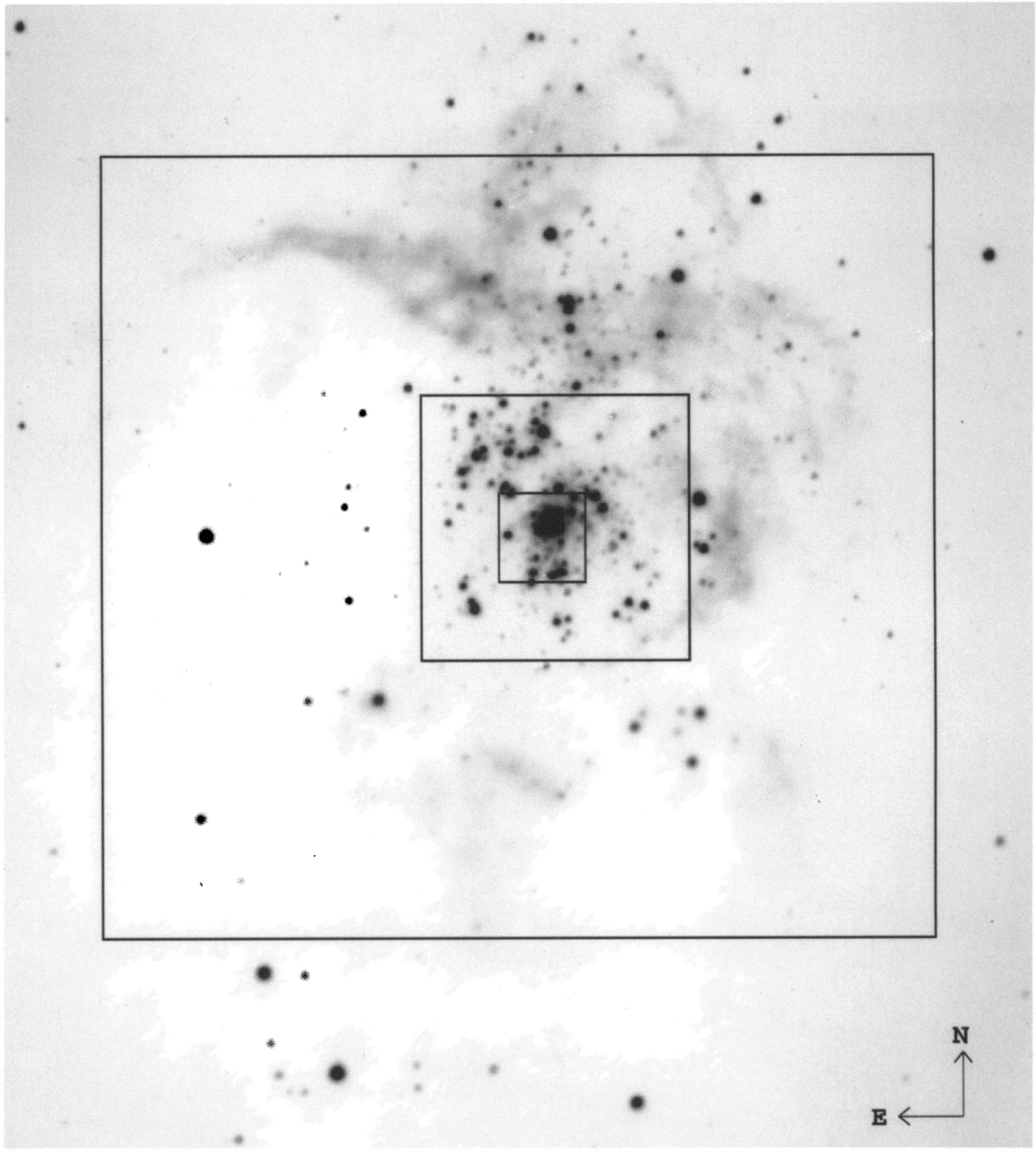

FIG. 1.—*V*-band image of 30 Dor, centered on R136, obtained by Parker (1992, 1993). Approximate locations of the three regions observed with *IUE*, using a drift-scan technique, are indicated. The middle box is 1′ on a side. Identification of the prominent stars in this image can be found in the paper by Moffat et al. (1987).

each wavelength by calculating a weighted sum over the instrumental profile. These procedures yield spectra with signal-to-noise ratios generally larger than those obtained with the standard *IUE* extraction routines. The spectra were then flux-calibrated with the 1980 absolute flux calibration for the SWP camera and corrections for the sensitivity degradation of the camera as a function of wavelength and time (Garhart 1992b) were applied. Temperature-dependent corrections to the camera sensitivity were determined to be less than 1% and therefore were not applied. The resulting spectra span the wavelength range 1100–2000 Å.

It is important to reiterate that the spectra obtained here are "spatially integrated" and correspond to the entire spatial regions covered by the scans, as if each region were moved to a distance such that it could fit entirely within the *IUE* aperture. The exposure times used to determine the absolute fluxes of the spectra, therefore, are not the total exposure times $t_{\rm total}$ for each observation, but rather the effective exposure times $t_{\rm eff}$ given by

$$t_{\rm eff} = \frac{w}{s}\left(1 - \frac{w}{l_s}\right) \quad (1)$$

$$\approx \frac{w}{N l_s}\, t_{\rm total}\,, \quad (2)$$

where w is the effective width of the aperture ($w = 9\farcs1/\sin\phi$, where ϕ is the position angle $\theta_{\rm pa}$ for the north-south scans and $90° - \theta_{\rm pa}$ for the east-west scans), s is the scan rate, l_s is the length of a single scan across the region, N is the number of scans in an observation, and $t_{\rm total}$ is the total exposure time for the entire observation. The effective exposure time is the mean time each spatial point in a scan remains within the aperture; it is given by the time required for the aperture to scan past a given point on the sky, multiplied by a correction term that accounts for the fact that points located within edges of width w at the beginning and end of each scan spend less time within the aperture than other points in the scan. For the 1′ × 1′ and 3′ × 3′ regions, the width of the aperture (and therefore the width of these edges) is small compared to the length of the individual scans, and consequently, the correction term is also small. Furthermore, for these two regions, the relative contributions of sources within the edges to the total integrated spectra are also small. (Sources on the edges of the scans contribute less to the integrated flux than those in the center. Unfortunately, it is impossible to correct for this nonuniform coverage and the subsequent differences in relative contributions to the total flux.) The reduced spectra for the three regions, smoothed to the *IUE* resolution of 6 Å using a five-point moving boxcar average, are presented in Figure 2*a*.

The spectra were dereddened using the average Galactic foreground extinction law given by Seaton (1979) and the average LMC UV extinction law determined by Fitzpatrick (1986). As discussed by Parker (1992), Parker & Garmany (1993), and Morris et al. (1993), there is some indication that the UV extinction law derived specifically for the 30 Dor region by Fitzpatrick (1986) may be too "steep" and its use may yield intrinsic spectra which are overcorrected for reddening; for this reason we chose to use the average LMC law instead. We adopted a foreground color excess of $E_{B-V} = 0.05$ (McNamara & Feltz 1980; Bessell 1991) and an internal LMC color excess of $E_{B-V} = 0.30$, as derived by Vacca (1991) from a spatially integrated optical spectrum of 30 Dor. The latter value is in good agreement with other determinations of the reddening within 30 Dor (Israel & Koornneef 1979; Fitzpatrick & Savage 1984). The dereddened spectra are presented in Figure 2*b*. The spectra were then normalized by dividing the observed wavelength range into four intervals, fitting a low-order Legendre polynomial to data sections considered to be free of stellar or interstellar lines (i.e., continua) within each interval, and then forcing the polynomial fits to match at the end points of the intervals. The dereddened spectra were then divided by the fitted curve. The normalized spectra were used in comparing the observed line profiles with the synthetic line profiles (see § 4.2).

3. SPECTRAL SYNTHESIS MODELS

3.1. *Description of the Models*

The spectral synthesis models used in our analysis are calculated with a computer code whose main features were described by Leitherer et al. (1992b) and Robert et al. (1993).

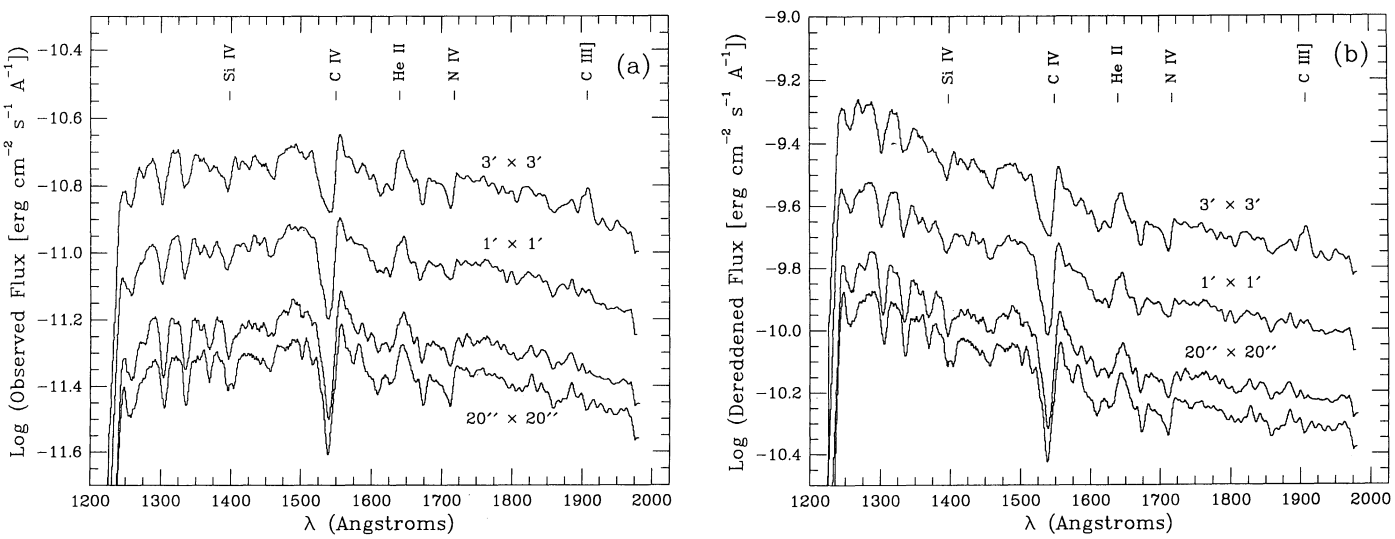

FIG. 2.—(*a*) Observed *IUE* spectra, smoothed to the resolution of 6 Å, for the three regions marked in Fig. 1. Prominent lines arising from the winds of hot stars are marked. (*b*) Intrinsic spectra for the same regions. The spectra have been dereddened using a Galactic foreground extinction law and the average LMC extinction law (see text).

The code incorporates a set of evolutionary tracks, a set of stellar atmosphere models, a library of stellar spectra, and a spectral type calibration (spectral type as a function of stellar effective temperature $T_{\rm eff}$ and luminosity L) which links the evolutionary and atmospheric models with the spectral library.

We employed the stellar evolution models of Maeder (1990) for high-mass stars, with masses of 15 $M_\odot$ and above, and those of Maeder & Meynet (1988) for lower mass stars. The metallicity of our spectral synthesis models is dictated by these evolutionary tracks. For $M \geq 15\ M_\odot$, evolutionary tracks for four metallicities (0.1 $Z_\odot$, 0.25 $Z_\odot$, $Z_\odot$, and 2 $Z_\odot$) are available. For masses below 15 $M_\odot$ only solar metallicity evolutionary models are available; however, metallicity effects in this stellar mass range are unimportant for the present study.

We interpolated the evolutionary tracks as a function of both mass and time. We used a mass interval of 1 $M_\odot$; we used a time interval of 10^4 yr, which is sufficiently small to resolve the shortest evolutionary phenomena of interest, such as the W-R phase. At each time step along each mass track, the effective temperature $T_{\rm eff}$ and bolometric luminosity $L_{\rm bol}$ were calculated. We then computed the desired stellar properties associated with $T_{\rm eff}$ and $L_{\rm bol}$. In the present study they are: the *current* stellar mass, surface gravity, and radius; the stellar spectral type derived from the stellar parameters and the evolutionary status; the monochromatic luminosity, L_λ, between 912 and 10000 Å with a typical resolution of about 100 Å; the number of ionizing photons emitted per second shortward of 912 Å, $N_{\rm LyC}$; and the synthetic UV line spectrum from 1250 to 1850 Å, constructed from empirical *IUE* high-dispersion spectra.

The spectral types of all pre–W-R stars were assigned according to Schmidt-Kaler's (1982) calibrations of $T_{\rm eff}$ and L. Classification of W-R stars is based on the surface abundances of hydrogen, helium, carbon, nitrogen, and oxygen predicted by the evolution models. This has the advantage of avoiding the temperature estimates for W-R stars, which are quite dependent on the exact temperature definition adopted. WC subtypes are identified according to the prescriptions given by Smith & Hummer (1988) and Smith & Maeder (1991). For the WN sequence we adopted the classification criteria of Conti, Leep, & Perry (1983).

Leitherer, Gruenwald, & Schmutz (1992a) outlined the methods used to model the stellar continua. Two sets of theoretical stellar atmospheres were used. The spectra of stars on the main-sequence and in pre–W-R phases were modeled with Kurucz's (1992) plane-parallel line-blanketed LTE atmospheres, with the same metallicity as that of the evolution model. The grid of Kurucz model atmospheres covers nearly the full range of temperatures, gravities, and metallicities required for our study. In a few instances, particularly for large values of $T_{\rm eff}$, we had to extrapolate the models to values of gravity lower than those provided. We verified that this had negligible consequences on the computed synthetic spectra. Cool stars with $T_{\rm eff} < 4000$ K were approximated by blackbodies. Their relative contribution to the integrated flux from the stellar populations discussed here is negligible.

The continua of stars with very strong winds (e.g., W-R stars) cannot be modeled with static, plane-parallel atmospheres. For those stars we used the expanding, spherically extended non-LTE models published by Schmutz, Leitherer, & Gruenwald (1992). The reader is referred to that paper for a description of the model atmospheres as well as a discussion of the details regarding the interface between the atmospheric and evolutionary models. The dynamic models of Schmutz et al. (1992) were used if the evolutionary models indicated the star had a hydrogen surface abundance $X_{\rm H} < 0.4$ by mass and $T_{\rm eff} > 25{,}000$ K; otherwise the static models of Kurucz (1992) were employed. These criteria coincide with the definition of a W-R star in Maeder's (1990) models. We emphasize that this convention is used only to denote regions in the Hertzsprung-Russell (H-R) diagram where high mass-loss rates and strong winds are found. Some fraction of the objects identified as W-R stars with these criteria may well be core-hydrogen–burning O stars with strong stellar winds. Our use of the model atmospheres of Schmutz et al. (1992) for these stars is justified, however, as these models are equally applicable to O stars with very strong winds as to W-R stars. Although the models of Schmutz et al. (1992) contain only He, the main opacity sources are due to free-free transitions and electron scattering, which to a first approximation are independent of metallicity. Therefore the chemical composition of the atmospheres has relatively little effect on the optical and near-UV fluxes. The same is true of course for the Kurucz models. We caution that the fluxes below 912 Å in the coolest models of Schmutz et al. may be overestimated due to the omission of line blanketing (Esteban et al. 1993). This should have little effect on our results, however.

The number of Lyman continuum photons produced per second by a star, $N_{\rm LyC}$, was calculated from either the static or the expanding model atmospheres. It should be noted that $N_{\rm LyC}$ is rather insensitive to the metallicity of the atmosphere due to the lack of significant metal opacities immediately below 912 Å. Individual W-R stars produce Lyman continuum photons at a rate comparable to the production rate from mid-O stars (Vacca 1991). However, as a result of the (generally) small W-R/O number ratio, the integrated Lyman continuum flux from a population of W-R stars is usually rather small (generally less than 10%) compared to that from the O star population.

In order to study the UV line profiles in the observed spectra, the spectral region between 1250 and 1850 Å was synthesized using a library of *IUE* UV spectra of O, B, and W-R stars. The appropriate spectra were selected from the library based on the spectral types previously assigned to each point in the H-R diagram. A detailed description of the spectral library has been given by Robert et al. (1993). The important new aspect, and significant improvement over existing spectral modeling codes, is the use of *high*-dispersion spectra for the hottest O and W-R stars, as opposed to the widely used *low*-dispersion libraries. The contributions of B stars to the integrated flux were calculated using *IUE* low-dispersion spectra. Stars of later spectral types are unimportant for the analysis of the spectral lines of interest here; their spectra were approximated by a featureless continuum. All spectra in our library are normalized to unity; we used the monochromatic luminosity between 1250 and 1850 Å derived from the atmospheric models to scale the line spectra to the required levels.

All stars used to construct the spectral library are located in the solar neighborhood, and consequently they have metallicities near $Z_\odot$. A sufficiently large set of high-resolution UV spectra of hot stars with nonsolar metallicities does not yet exist. (Collection of such data with the *HST* is currently being carried out by some of us.) For the present, we have to make use of a solar metallicity line-profile library and be aware of the errors possible when applying it to star-forming regions in the slightly metal-deficient environment of the LMC.

No attempt has been made to remove interstellar lines from the library spectra. Isolated low-ionization resonance lines, such as O I λ1300, are not formed in hot stars and are easily recognizable as interstellar by their line widths. Some lines, such as Si II λ1527, are predominantly of interstellar origin but sometimes blend with nearby stellar features (in this case with blueshifted C IV λ1550). In most instances, they can be removed with deblending techniques. However, high-ionization lines, such as Si IV λ1400, can originate in both stars and the interstellar medium. In the spectra of O main-sequence stars, for example, the strengths of the interstellar and photospheric Si IV absorption lines can be comparable (see Leitherer & Lamers 1991), and it is virtually impossible to subtract the interstellar component. For the sake of consistency, then, no interstellar lines were removed from the UV spectra in the spectral library.

Finally, the synthetic spectra computed with our models do not include any contributions to the continuum from free-free, bound-free, or two-photon emission. Nor do they include any line emission from photoionized or shocked gas within the observed regions. Test calculations indicate that the predicted continuum levels will increase by only $\sim$10% at early times if the nebular continuum flux is included in the models. This will not significantly affect our conclusions based on the continuum levels (see § 4.1). Although the nebular continuum flux will also dilute the stellar UV lines somewhat, we do not find the effect to be significant.

3.2. *Application to 30 Dor*

The theoretical spectra synthesized with our models depend critically on the assumptions made regarding the star formation history and the stellar mass spectrum. For this analysis we investigated two star formation scenarios: (1) the "continuous burst" scenario, in which stars form continuously at a constant rate, and (2) the "instantaneous burst" scenario, in which stars of all masses form instantaneously with no subsequent star formation. Instantaneous and continuous bursts are extreme assumptions, and we expect them to bracket the actual star formation history in 30 Dor. Because of the large number of free parameters involved, spectral synthesis models can never yield truly unique solutions, and it is certainly possible to obtain a very close match to the observed spectra with highly complicated star formation histories. However, we attempted to reproduce the observations with the simplest assumptions possible.

A power-law shape for the IMF was adopted:

$$\phi(M) = \frac{dN}{dM} = CM^{-\alpha}, \tag{3}$$

where $\phi(M)$ is the number of stars per unit mass interval dM between M and $M + dM$, N is the total number of stars present, and C is a normalization constant. We chose the canonical Salpeter (1955) value for the power-law index, $\alpha = 2.35$. This value of the IMF "slope" is in reasonable agreement with the results of several independent studies of the IMF in 30 Dor (Parker 1992; Parker & Garmany 1993; Malumuth & Heap 1994). Steeper and shallower slopes were considered, but variations in α of ± 0.5 do not lead to significantly different UV spectra (cf. Robert et al. 1993; Leitherer & Heckman 1995). Therefore, we do not discuss variations of the IMF slope in this paper. We do discuss, however, the influence of the upper cutoff mass M_{upp} on the synthetic UV spectra. Varying the upper cutoff mass is an even more drastic way of modifying the IMF than changing the slope.

The lower cutoff mass M_{low} was held at 1 $M_\odot$. As long as $M_{low} < 5\ M_\odot$, the lower cutoff mass enters only as a normalization constant for the synthetic spectra and has almost no effect on the line spectra and the continuum slopes. This is simply a consequence of the fact that the most effective contributors to the UV spectra are stars with masses substantially larger than 5 $M_\odot$. Therefore, our study cannot address the important issue of the masses of the least massive stars formed in the 30 Dor region.

We generated a series of models for the two star formation scenarios, for a series of ages τ between 1 and 10 Myr, two values of the metallicity Z (0.25 $Z_\odot$ and $Z_\odot$), and values of the upper cutoff mass M_{upp} of the IMF of 30, 40, 50, 60, 80, 100, and 120 $M_\odot$. For each age τ and metallicity Z we computed the synthetic spectrum from a stellar population generated according to the star formation history and the parameters of the IMF chosen for the model. The total numbers of stars of various spectral types, as well as the relative fractions of specific subtypes, such as W-R/O, WC/WN, etc., were also calculated at each age. These quantities were directly compared with the observed values (see § 4.3). We also investigated the effects of the metallicity on the synthesized spectrum. Particular emphasis was placed on models with $Z = 0.25\ Z_\odot$, as the metallicity of the 30 Dor region is $\sim$0.30 $Z_\odot$ (Dufour 1984; Mathis et al. 1985; Rosa & Mathis 1987; Vacca 1991).

All our models were normalized to reproduce the N_{LyC} estimated for the regions covered by the *IUE* observations. The choice of N_{LyC} values to use in the normalization is a difficult one. Values derived from different data sets with different methods, covering different spatial regions, vary considerably, and it is not immediately clear which are the most appropriate for our analysis. Here we examine three recent estimates of N_{LyC} in detail.

A reanalysis of the Hα images of the 30 Dor region obtained by Kennicutt & Hodge (1986) yields observed Hα fluxes of 7.8×10^{-10} and 6.7×10^{-9} ergs cm^{-2} s^{-1} for our 1′ × 1′ and 3′ × 3′ regions, respectively (R. C. Kennicutt 1994, private communication). (For reasons discussed below, we restricted our analysis to these two regions.) With the color excesses and reddening laws we adopted, these Hα fluxes correspond to Lyman continuum photon luminosities of 1.80×10^{50} and 1.55×10^{51} photons s^{-1} for the 1′ × 1′ and 3′ × 3′ regions, respectively. However, values of N_{LyC} deduced from Hα images depend sensitively on the spatial distribution of the emitting gas, which may be less centrally concentrated than the stars within the region, and on the assumption that the gas within the region is completely ionization bounded. In the relatively small inner regions of the 30 Dor Nebula which we are studying, this latter assumption may not be valid, and the measured Hα fluxes may yield underestimates of the true ionizing continuum luminosity in the region (Mills, Turtle, & Watkinson 1978). For these reasons, the values of N_{LyC} given above may not accurately reflect the ionizing continuum radiation produced by the embedded stars.

Of the numerous spectroscopic and photometric studies of the hot stars within 30 Dor, perhaps the most extensive and complete surveys of the region have been carried out by Parker (1992, 1993) and Malumuth & Heap (1994). Parker (1992, 1993) acquired several ground-based *UBV* CCD images of a $\sim$7′ × 7′ region centered on R136. These photometric data were combined with optical spectroscopy of the bluest stars to confirm their spectral types. With these data he took a "census" of the stellar content within the region, determining

the number of massive stars in the region and estimating the slope of the mass function (Parker & Garmany 1993). Parker (1992) also calculated the Lyman continuum flux from the stars he identified on his images. By interpolating in Parker's (1992) Figure 4.11, which presents the cumulative value of log N_{LyC} as a function of the distance from R136, and correcting for the rectangular geometry of the regions observed with *IUE*, we find $N_{LyC} = 1.26 \times 10^{51}$ s^{-1} in the 1′ × 1′ region and $N_{LyC} = 2.51 \times 10^{51}$ s^{-1} in the 3′ × 3′ region. Although the values of N_{LyC} derived from Parker's data are directly tied to the actual distribution of stars in the regions, the severe crowding in R136 introduces errors in any attempt to determine reliable photometric magnitudes, spectral classifications, etc., from ground-based CCD images of the cluster. Thus, the values of N_{LyC} derived by Parker (1992) for this central cluster certainly underestimate the contribution from unresolved components. Furthermore, Parker's values do not include contributions from W-R stars, although he estimates that these objects contribute less than 10% of the total Lyman continuum flux.

Malumuth & Heap (1994) performed an analysis, similar to that of Parker (1992, 1993), on *UBV* images obtained with *HST* of a 35″ × 35″ region centered on R136a. Using these images and an evolutionary model for the central cluster presented by Malumuth & Heap (1994), E. M. Malumuth (1994, private communication) estimates that the stars within the 35″ × 35″ region centered on R136a produce 1.86×10^{51} Lyman continuum photons s^{-1}; this value is presumably a lower limit, as it excludes the contribution from the known W-R stars in the region. This estimate of N_{LyC} is already 1.5 times larger than that determined by Parker (1992), and over 10 times larger than that derived from the Hα measurements of Kennicutt & Hodge (1986), even though it corresponds to a region only one-third the size of the 1′ × 1′ region observed with *IUE*.[4] However, the results of Malumuth & Heap (1994) are based on *UBV* photometry alone, without the aid of spectra to confirm the spectral types (and hence effective temperatures) suggested by the colors or absolute *B* magnitudes. Furthermore, Malumuth & Heap (1994) assumed that *all* of the objects they identified were located on a single isochrone calculated for an evolutionary time of 3 Myr. Until spectra can be obtained for these stars, the spectral classifications for most of these objects will remain unknown or uncertain. Consequently, the N_{LyC} value obtained by Malumuth & Heap (1994) must also be considered rather uncertain.

Given the various uncertainties in these estimates of the Lyman continuum luminosities for the regions of 30 Dor observed with *IUE*, we chose to use the N_{LyC} values derived from Parker's (1992) data. Although probably underestimates, these values are intermediate between the larger values implied by the results of Malumuth & Heap (1994) and the smaller values of Kennicutt & Hodge (1986). In § 4.1 we discuss the effects of changing N_{LyC} by a factor of 2 on our results.

In addition to the uncertainty in N_{LyC}, there are uncertainties in our analysis resulting from an imprecise knowledge of the exact position of the *IUE* aperture at the start of each observation, and the fact that the regions covered by the *IUE* observations are neither circular nor perfectly square. The effect of the former uncertainty on the observed spectra can be clearly seen in Figures 2*a* and 2*b*. The two spectra for the 20″ × 20″ region differ by ~23%, simply as a result of small differences in the initial pointing positions of *IUE*. The spectra corresponding to the larger 1′ × 1′ and 3′ × 3′ regions should be less affected by these errors, however. Furthermore, because the width of the aperture (and, therefore, the beginning and ending edges of the individual scans) is half the length of the scan for the observations of the 20″ × 20″ region, the relative contributions of the various sources within the region to the total integrated spectra are highly nonuniform. For the observations of the 1′ × 1′ and 3′ × 3′ regions, the edges are much smaller than the individual scan lengths and most of the sources within these regions contribute to the integrated spectra with equal weight. We therefore excluded the spectra for the 20″ × 20″ region from any further quantitative analysis. Additional uncertainties in our results arise from the small uncertainties (less than ~10%) in the *IUE* absolute flux calibration and the correction factors for the degradation of the camera sensitivity as a function of time. Uncertainties in the color excess and reddening law used to deredden the spectra have a much larger effect on our results. We briefly discuss these effects below (§ 4.1).

4. RESULTS

4.1. *The UV Continuum Spectra*

We first discuss the analysis of the UV continuum spectra of 30 Dor recorded during our observations with *IUE*. In Figure 3, a series of synthetic spectra computed from instantaneous burst models with ages of 1–4 Myr is compared with the observed spectra from the 1′ × 1′ and 3′ × 3′ regions. The observed spectra have been dereddened as described in § 2. The models presented have been computed for two metallicities, $Z = 0.25\ Z_\odot$ and $Z_\odot$, with an upper cutoff mass of 100 $M_\odot$ (consistent with the upper mass values determined by Parker 1992). Although the individual theoretical stellar continuum fluxes are not greatly affected by metallicity differences, the total continuum flux level produced by a synthesized stellar population does vary with metallicity, as Figure 3 reveals. This is purely a result of the dependence of the stellar evolution models on metallicity. The zero-age main sequence (ZAMS) is shifted to higher T_{eff} in models with lower metal content. Therefore the model stars initially emit somewhat more Lyman continuum photons, and fewer stars are required to produce the observed N_{LyC}. Consequently, the continuum level of the spectra with $Z = 0.25\ Z_\odot$ is lower than that at $Z = Z_\odot$. This explanation is valid only during early evolutionary phases. The situation may be reversed at later times, as *Z*-dependent stellar evolution may, under certain conditions, lead to lower mean effective temperatures in metal-poor populations as compared to metal-rich populations.

The continuum levels of the synthetic spectra increase with the age of the burst. Stars become cooler as they evolve off the ZAMS, and eventually they reach the terminal point of their evolution. This generally leads to a reduction in the output rate of Lyman continuum photons per star as a function of time. Since each model is normalized to the same total number of Lyman continuum photons per second, older models require a larger number of stars of any initial mass to produce the same N_{LyC}. The increased continuum levels at later times are therefore due to the increased number of stars which are necessary to produce the observed N_{LyC}.

[4] We note that radio observations yield a similar "excess" of ionizing photons with respect to the Hα observations for the 3′ × 3′ region. Israel & Koornneef (1979) reported a value of N_{LyC} of 1.2×10^{52} ionizing photons s^{-1} for the central 3′ × 3′ region of 30 Dor derived from observations at 5 GHz. This value is ~10 times that determined from the Hα measurements of Kennicutt & Hodge (1986).

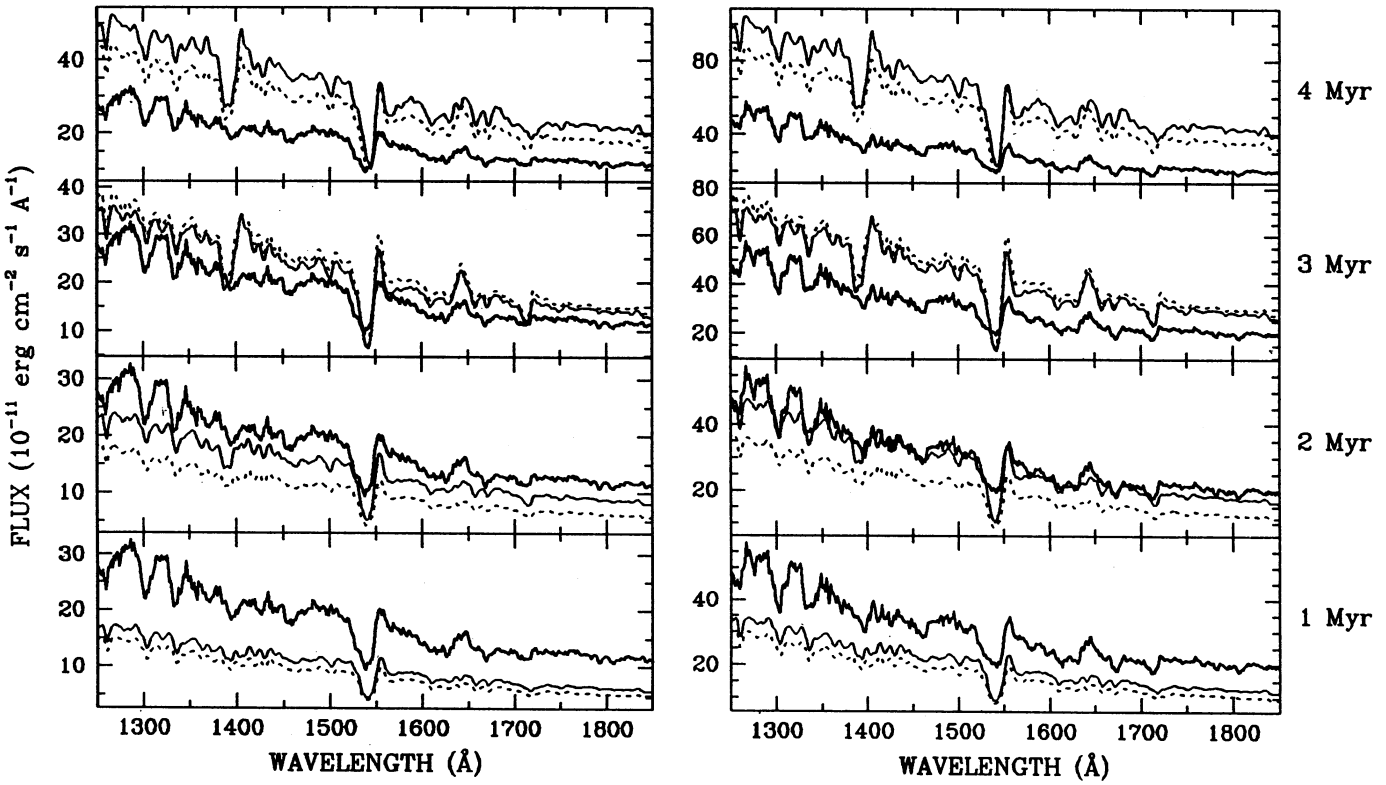

FIG. 3.—Observed (*thick solid line*) and synthetic (*thin solid line*, $Z = Z_\odot$; *dashed line*, $Z = 0.25\ Z_\odot$) UV spectra of 30 Dor. *Left:* Spectral time series for the 1′ × 1′ region; *right:* spectral time series for the 3′ × 3′ region. The synthetic spectra were calculated assuming an instantaneous burst with $\alpha = 2.35$, $M_{low} = 1\ M_\odot$, and $M_{upp} = 100\ M_\odot$. Each model is constrained at all times to produce $N_{LyC} = 1.26 \times 10^{51}$ s^{-1} and 2.51×10^{51} s^{-1} ionizing photons for the 1′ × 1′ and 3′ × 3′ regions, respectively. The noise in the synthetic spectra is due to the noise present in the stellar spectra included in the spectral library.

The observed continuum fluxes in the *IUE* spectral range provide stringent limits on the ages of the burst episodes in the central 1′ × 1′ and 3′ × 3′ regions of 30 Dor. By $\tau \approx 2.5$ Myr after an instantaneous burst, a significant number of stars with initial masses $M \gtrsim 50\ M_\odot$ have left the main sequence, and the reduced production rate of Lyman continuum photons can be compensated only by a larger number of less massive O stars. After ~2.5–3 Myr, the theoretical continuum level, due primarily to these numerous less massive O stars, is higher than the observed *IUE* fluxes. As seen in Figure 4, the results are qualitatively similar for the continuous burst scenario. Again, the flux level increases with age, and after ~6–8 Myr the theoretical continua are higher than the observed levels. The upper limit for the burst age is higher for a continuous burst than for an instantaneous burst. In a continuous burst, new generations of massive stars continue to form when the first generation of O stars begins to leave the main sequence, and the decline in N_{LyC} can be partially compensated by newly formed very massive stars ($M > 50\ M_\odot$), until $\tau \approx 6$ Myr. At that time, an equilibrium is reached between the formation and destruction of these very massive stars. However, the birth and death of less massive O stars are not yet in equilibrium at this time; these O stars do not achieve an equilibrium population until $\tau \approx 10$ Myr. Therefore, for ages $\tau > 6$ Myr, a larger number of less massive O stars is required to produce the observed N_{LyC}, and the UV continuum level rises correspondingly. The general result is that the theoretical continuum level increases more slowly with burst age in the continuous burst scenario than in the instantaneous burst scenario.

From the model results presented in Figures 3 and 4 we conclude that, for an IMF slope of $\alpha = 2.35$ and an upper cutoff mass of $M_{upp} = 100\ M_\odot$, the age of the starburst episode in the central regions of 30 Dor must be less than ~3 Myr for an instantaneous burst scenario or less than ~7 Myr for a continuous burst scenario. The *lower* age limit is essentially unconstrained by the observed continuum levels. Since O stars experience little evolution in T_{eff} and L_{bol} during the first 2 Myr of their lives, the theoretical continuum fluxes are not very sensitive to the burst age until after $\tau \approx 2$ Myr. By decreasing the value of M_{upp}, the synthetic continuum levels can be made to match the observed continuum levels at arbitrarily young burst ages (see below).

So far, we have restricted our discussion to the case of a fixed upper cutoff mass of 100 $M_\odot$ and a variable burst age τ. In Figure 5 we investigate the effects on the synthetic spectra calculated for an instantaneous burst scenario when M_{upp} is varied and the burst age is fixed at $\tau = 2.5$ Myr. As this figure reveals, the lower M_{upp}, the higher the theoretical continuum level. The explanation for this is the same as that for the higher continuum with older burst age: if the most massive stars are absent, a larger number of less massive O stars are required to produce the observed N_{LyC}. The effect is particularly dramatic if M_{upp} is as low as 30 $M_\odot$. In this case, even models with a burst age of 1 Myr are unable to match the observations; such a value of M_{upp} would clearly be inconsistent for any burst age. For the continuous burst scenario, the minimum M_{upp} which is still consistent with the *IUE* observations depends on the assumed burst age. The older the burst, the higher M_{upp} must

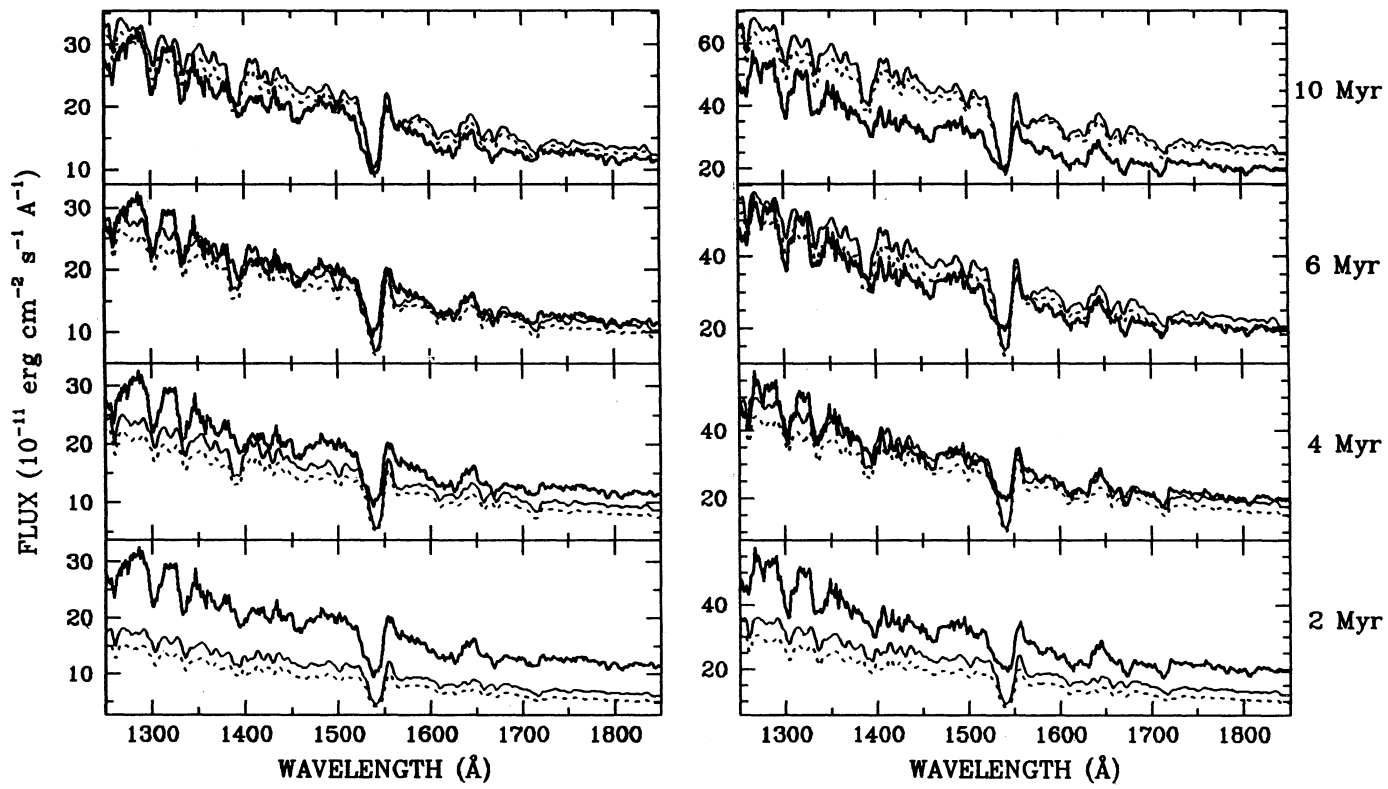

FIG. 4.—Same as Fig. 3, for a continuous burst

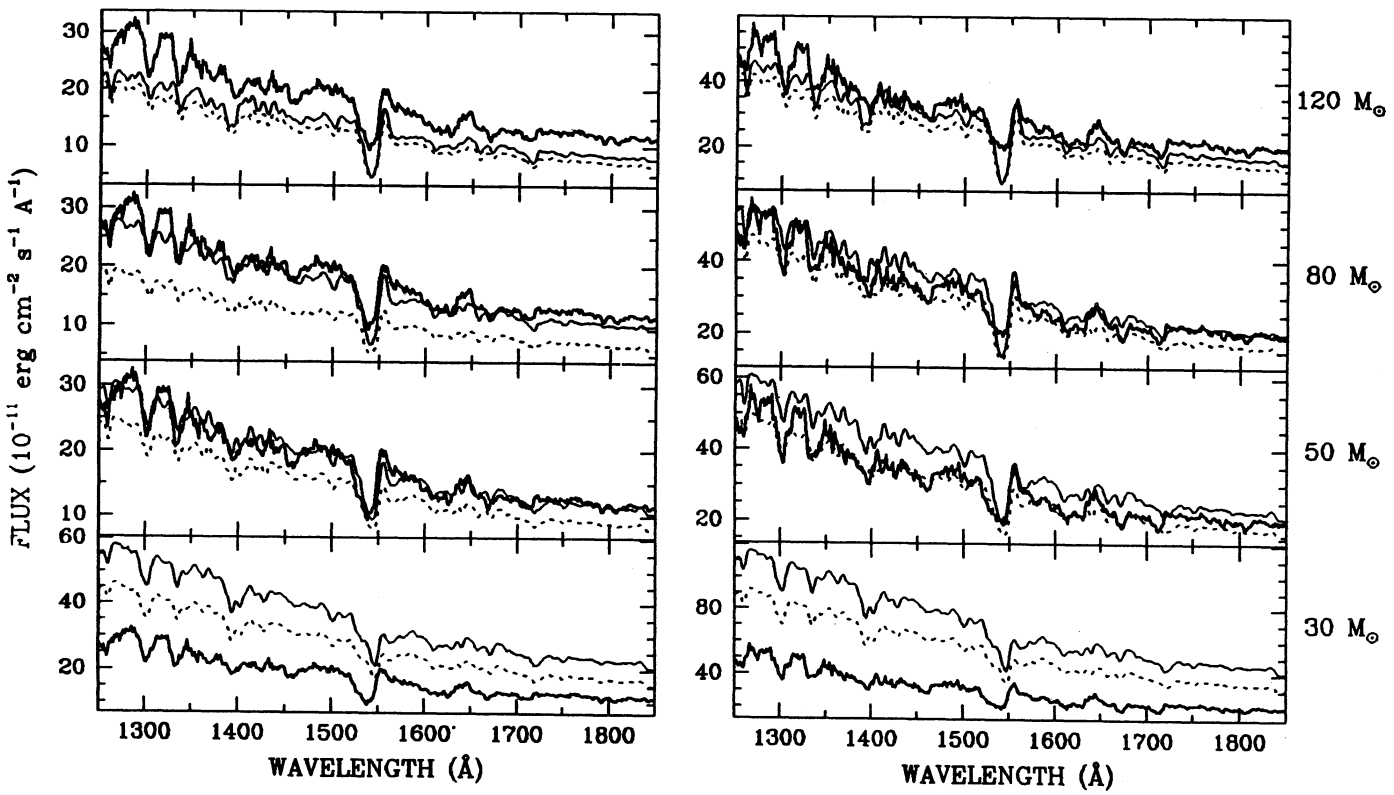

FIG. 5.—Observed (*thick solid line*) and synthetic (*thin solid line*, $Z = Z_\odot$; *dashed line*, $Z = 0.25\ Z_\odot$) UV spectra of 30 Dor. *Left:* 1′ × 1′ region; *right:* 3′ × 3′ region. The synthetic spectra were calculated assuming an instantaneous burst with $\alpha = 2.35$ and $M_{low} = 1\ M_\odot$ and an age of $\tau = 2.5$ Myr. The effect of varying M_{upp} on the synthetic spectra is demonstrated.

be in order to reproduce the observed N_{LyC}. We find that $M_{upp} \simeq 100\ M_\odot$ if we restrict the burst age to $\tau < 7$ Myr. We note here that, in either star formation scenario, the theoretical continuum level is fairly insensitive to the exact value of the upper cutoff mass when $M_{upp} > 80\ M_\odot$. Due to the power-law shape of the IMF, very few stars have masses greater than $\sim 100\ M_\odot$; their *total* contribution to N_{LyC} is negligible, despite the high photon output *per star*.

The limits on τ and M_{upp} given here are strengthened by the fact that the values of N_{LyC} derived from the results of Parker (1992) are most likely *lower* limits to the true values. For either burst scenario, an increase in the observed value of N_{LyC} results in an increase in the best-fitting upper cutoff mass value derived from a model with a given burst age. Similarly, an increase in N_{LyC} results in a decrease of the value of the best-fitting burst age for a model with a given upper cutoff mass. Thus, the values of M_{upp} found here are probably lower limits, while the values of τ are most likely upper limits.

It should be noted that, for an instantaneous burst model, M_{upp} refers to the *present-day* value of the upper cutoff mass. At times greater than ~ 3.3 Myr after the burst, the most massive stars begin to die and the upper cutoff mass drops steadily and rapidly. Thus, for any instantaneous burst model with a burst age greater than ~ 3.3 Myr, the *present-day* value of the upper cutoff mass may be substantially lower than the *initial* value of the upper cutoff mass. For example, at an age of $\tau = 4$ Myr after an instantaneous burst, none of the stars produced in the burst with initial masses $M \gtrsim 60\ M_\odot$ remain. Since the effects of these massive stars are no longer observable in the synthetic spectra (because they are not being continuously replaced by newly formed stars), the models are not sensitive to values of $M_{upp} \gtrsim 60\ M_\odot$ at this time. *This does not imply, however, that these massive stars did not once exist within the region.* The presence of W-R stars, for example, is always an indication that very massive stars were once present in a star-forming region. Of course, the present-day value of the upper cutoff mass is always equal to the initial value in a continuous burst scenario. Furthermore, as long as the burst age is shorter than the lifetime of the initially most massive star formed during an instantaneous burst, the initial value of the upper cutoff mass will be the same as the present-day value. For the specific case of 30 Dor, a burst age of ~ 3 Myr implies that there is no ambiguity in the upper cutoff mass derived from the instantaneous burst models.

From the discussions above, it should be clear that fits to the observed UV continua alone cannot provide tight constraints on *all* the parameters describing a starburst episode simultaneously. For example, during the early phases of a burst (i.e., ages less than or comparable to the evolutionary timescale of the most massive O stars, or ~ 3–5 Myr), an instantaneous burst and a continuous burst produce similar spectra (continuum level and slope, and line features). In fact, it is extremely difficult to distinguish between the two burst scenarios on the basis of spectra alone at these times. This is due to the fact that the properties of O stars vary little during their evolution until they reach the end of their main-sequence lifetimes. The absolute numbers of O and W-R stars in a region, however, provide additional constraints on the models and may aid in distinguishing between the two burst scenarios. Only by considering all three sets of observations (continuum spectra, line spectra, and numbers of stars) can a consistent set of burst parameters be determined.

The models for the UV continua do, however, provide some (limited) confirmation of the color excesses we adopted. Although the value of the total color excess we used ($E_{B-V} = 0.35$ mag) agrees with other determinations reported in the literature, Parker (1992) and Parker & Garmany (1993) find a significantly larger color excess of 0.44 mag from their stellar photometry. Dereddening the observed spectra with this value of E_{B-V} increases the continuum levels of the intrinsic spectra by about a factor of 2. It also results in slopes for the intrinsic spectra which are close to the steepest values the models can produce. Nevertheless, we attempted to fit our models to these versions of the corrected spectra. With higher continuum flux levels, the best-fitting evolutionary age τ (for a given M_{upp}) must increase; similarly, for a given τ, the value of M_{upp} must decrease. For an instantaneous burst scenario, a model with $\tau = 5$ Myr and $M_{upp} = 60\ M_\odot$ provides a reasonable fit to the general continuum levels. However, the model does not reproduce the slopes of the dereddened continua. For a continuous burst scenario, the only model which adequately fits the data yields $\tau = 5$ Myr and $M_{upp} = 30\ M_\odot$; models with $M_{upp} > 30\ M_\odot$ never produce enough continuum flux to match the dereddened spectra. Because W-R and massive O stars are known to exist in 30 Dor, an upper cutoff mass of $30\ M_\odot$ is clearly excluded. Based on these results we suggest that the color excess derived by Parker (1992) and Parker & Garmany (1993) may be an overestimate.

4.2. *The UV Line Spectra*

We now compare the lines observed in the UV spectra of 30 Dor, in particular the Si IV λ1400, C IV λ1550, and He II λ1640 features, with the synthetic lines computed for an instantaneous and a continuous burst with solar metallicity $Z_\odot$. Although the synthetic line strengths and profiles vary as a function of metallicity, it is not possible to produce synthetic lines at other metallicity values yet, since, as mentioned earlier, our spectral library contains stars located only in the solar neighborhood. To facilitate the comparison between the observed and synthetic line profiles we normalized the continuum levels to unity using the procedure outlined in § 2; by removing the overall continuum shapes the comparisons can be carried out much more objectively. We also degraded the wavelength resolution of the synthetic spectra to match the resolution of the low-dispersion *IUE* spectra (~ 6 Å).

Because the observed profiles of the UV lines of Si IV λ1400, C IV λ1550, and He II λ1640 are strongly dependent on the massive star population (Leitherer & Lamers 1991), these lines provide important constraints on the age of the starburst episode and the upper cutoff mass of the IMF. The Si IV λ1400 and C IV λ1550 lines are resonance doublets which may be formed in stellar photospheres and stellar winds (e.g., Walborn & Panek 1984a, b), as well as the interstellar medium. The spectra of evolved massive stars exhibit Si IV lines with strong P Cygni profiles and large displacements of the absorption components of the profiles to shorter wavelengths (blueshifts) due to the Doppler effect in the high-velocity, dense stellar winds. Because of the large optical depth of the C^{+3} ion in the stellar wind, the C IV line exhibits a strong P Cygni profile even in the spectra of massive main-sequence stars. The width of the C IV line is narrower in the spectra of massive supergiant stars than in the spectra of main-sequence stars because of the reduced Doppler shift in the relatively slower wind. In contrast, collisional broadening in the photospheres of B stars yields broad, unshifted Si IV and C IV absorption profiles in the spectra of these stars. The He II line is a recombination line observed to have a broad emission profile in the spectra of massive stars with fast and dense winds, such as W-R stars. It is

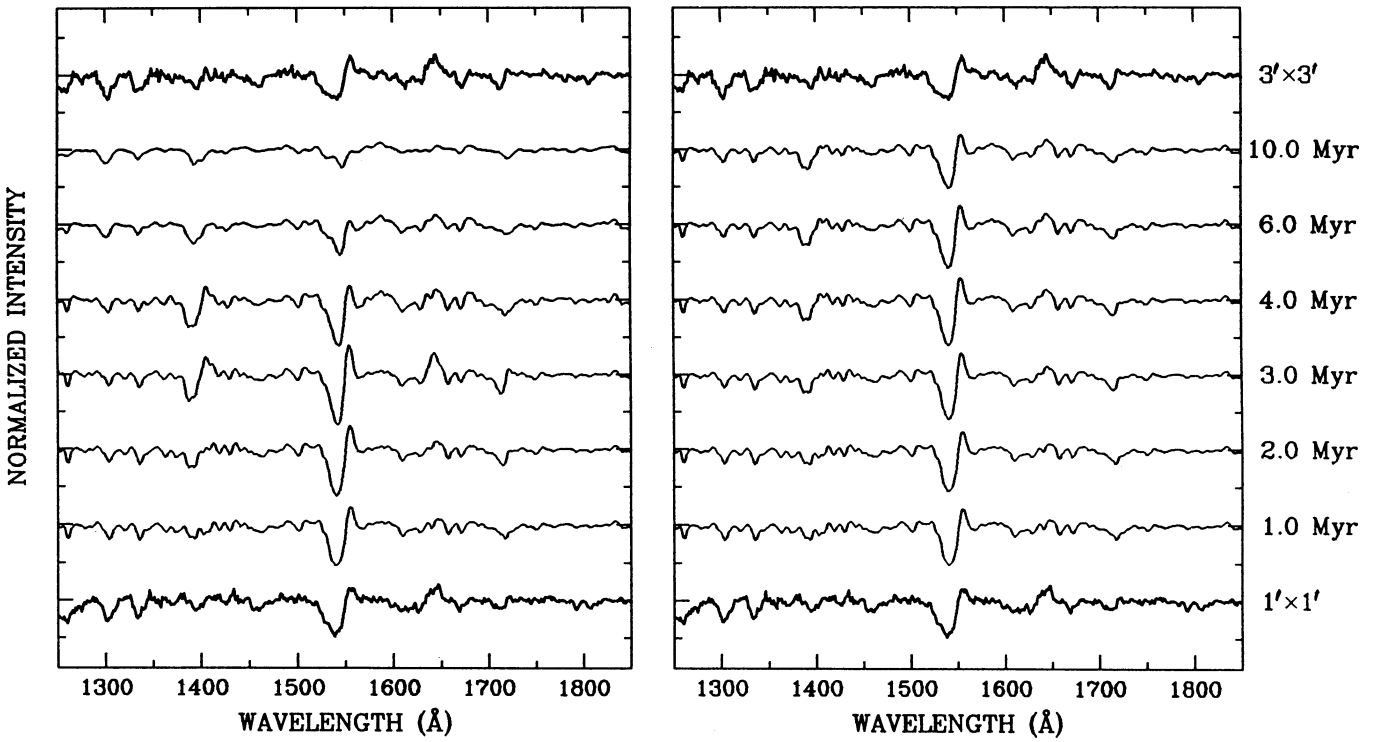

FIG. 6.—Observed (*thick lines at top and bottom*) and synthetic (*thin lines*) line spectra of 30 Dor. *Left:* Spectral time series for an instantaneous burst; *right:* spectral time series for a continuous burst. Model parameters are $Z = Z_{\odot}$, $\alpha = 2.35$, $M_{low} = 1\ M_{\odot}$, and $M_{upp} = 100\ M_{\odot}$.

clear, then, that the observed profiles of the Si IV, C IV, and He II lines in an integrated spectrum of a starburst region will exhibit strong variations depending on the initial stellar content and the age of the star-forming episode. These lines can therefore be used as sensitive diagnostics of the massive star population.

Figure 6 shows a time series of synthetic UV line spectra computed for instantaneous and continuous burst models with $M_{upp} = 100\ M_{\odot}$. The observed spectra for the $1' \times 1'$ and $3' \times 3'$ regions are also displayed at the bottom and top, respectively, of the figure for comparison. In the case of an instantaneous burst, we see strong variations in the synthesized profiles of the Si IV, C IV, and He II lines as a function of time. Other synthetic lines of interstellar origin, such as O I λ1302 and C II λ1335, have profiles which are constant in time and which coincide well in wavelength with the observed interstellar features in the 30 Dor spectra. (The differences in strength between the observed and synthetic interstellar lines are due to the fact that the column depth of interstellar material along the line of sight toward 30 Dor is different from that toward the stars included in the spectral library.) The Si IV line develops a strong P Cygni wind profile as soon as O supergiants appear, after ~ 3 Myr. At that time, the absorption component of Si IV exhibits a strong blueshift of hundreds of km s^{-1}. At later times ($\tau \geq 5$ Myr) the Si IV line exhibits a broad absorption profile, but is no longer blueshifted, as B stars become the dominant contributors to the integrated profile. The C IV line increases in strength and becomes narrower when O supergiants become important contributors to the integrated spectrum of the cluster ($\tau \simeq 3$ Myr). Again, as B stars begin to dominate the population, the C IV line becomes a broader, unshifted absorption line. He II evolves from a narrow absorption to a broad emission line, which weakens and eventually disappears entirely. The strongest He II emission, which occurs at an age ~ 3 Myr, corresponds to a peak in the number of W-R stars present in the population. Before this time, the photospheres of O main-sequence stars account for the narrow absorption line. In the continuous burst scenario, less variation is seen in all three of the lines after 3 Myr due to the equilibrium between the formation and death of the most massive stars.

The observed profiles of the Si IV and C IV lines provide an important constraint on the age of the starburst episode in 30 Dor. For the $1' \times 1'$ region, the Si IV profile yields an age smaller than ~ 3 Myr, or larger than ~ 5 Myr, in the case of an instantaneous burst with $M_{upp} = 100\ M_{\odot}$. An upper limit of ~ 3 Myr is obtained from the Si IV line in the case of a continuous burst. Although the strength of the observed Si IV line is not always well reproduced by the models (as might be expected since there is an interstellar contribution to the synthetic line), the pure absorption profile seen in the spectrum of the $1' \times 1'$ region can be produced in the synthetic spectra only during these restricted sets of times.[5] For an instantaneous burst model, the observed C IV line profile in the spectrum of the $1' \times 1'$ region places an upper limit on the age of the burst of ~ 5 Myr, while the He II line shape yields an upper limit of $\tau \lesssim 10$ Myr. The C IV and He II line profiles yield no useful constraints on the burst age in the continuous burst scenario.

Combining these results, we find that the overall population in the $1' \times 1'$ region centered on R136 can be characterized by an age with an upper limit of $\tau \lesssim 3$ Myr. This conclusion is

[5] We should point out that, based on high-resolution UV observations of interstellar absorption lines along the line of sight to SN 1987A (Blades et al. 1988), we do not expect interstellar absorption to have a significant effect on the *observed* Si IV, C IV, and He II line profiles.

based on the comparison of the observed spectrum with spectra synthesized from models computed for $Z = Z_\odot$. Ideally, in the case of 30 Dor, a lower metallicity model should be computed, but there is no spectral library available yet for metallicities other than solar. To a first approximation, however, our results are independent of the metallicity of the stars whose spectra are included in the spectral library. Although the *strength* of the stellar emission and absorption lines does depend on the metallicity, the shape and blueshift of the absorption profiles (i.e., the *radial velocity* in the stellar wind) are far less sensitive to metallicity effects (e.g., Garmany & Conti 1985). Therefore, based on observations of individual stars with lower metallicity, we believe the current models will not lead us to underestimate the age of a young burst, like that which occurred in 30 Dor, by more than 1 Myr due to metallicity effects. On the other hand, the nearly perfect agreement between the observed and theoretical line *strengths* in the $1' \times 1'$ spectrum is probably somewhat fortuitous.

We find it more difficult to obtain a good fit to the observed UV line spectrum of the $3' \times 3'$ region. Based primarily on the observed velocity shifts of the absorption components of the Si IV and C IV lines, an age of ~ 3 Myr is again indicated. For the reasons given above, we expect the velocity shifts, rather than the line strengths, to provide the best constraints on the burst age. Nevertheless, we cannot dismiss the fact that the line strength of C IV is not well reproduced by any model we generated. Even with a lower metallicity library, we do not expect that the fit to the C IV line would be completely satisfactory since both the emission and the absorption part of the profile should be equally reduced at lower metallicity. It is possible that the integrated spectrum from the $3' \times 3'$ region is produced by two stellar populations resulting from two bursts of star formation: a relatively young population produced in a very recent burst, as found for the $1' \times 1'$ region, superposed on an older population. The effect of the older burst population would be to dilute the lines without greatly affecting the velocity shift of the absorption components. However, because of the large number of free parameters in the models (age, upper cutoff mass, IMF slope, and metallicity), as well as the inherent limitations of the models themselves (e.g., the neglect of the nebular continuum flux and emission lines and the lack of nonsolar spectral libraries), we did not pursue the modeling of the UV lines in the spectrum of the $3' \times 3'$ region using multiple bursts. At present, our attempts to model the spectrum of the $3' \times 3'$ region are not completely successful.

Finally, we consider the influence of the upper cutoff mass on the synthesized line profiles. In Figure 7, we have plotted the synthetic spectra calculated for various values of upper cutoff mass for the instantaneous and the continuous burst scenarios and a burst age of $\tau = 2.5$ Myr. The observed spectra from the two regions are again shown at the top and bottom of the plot to facilitate comparisons with the models. The best fits to the observed spectra require $M_{upp} > 50\ M_\odot$ for both the instantaneous and the continuous burst models. Massive O stars ($M > 50\ M_\odot$) are important contributors to the integrated Si IV and C IV profiles, and their presence is immediately recognizable in a synthetic spectrum. If stars more massive than $50\ M_\odot$ are not produced in the burst, the P Cygni shape of the C IV line, and to some degree that of the Si IV line, are weakened (i.e., the line intensities and the velocity shifts are reduced). The He II emission line is also reduced, primarily because fewer W-R stars are present. The large blueshifts observed for the C IV absorption component places a robust lower limit on M_{upp}. *Low values such as* $M_{upp} = 30\ M_\odot$ *can be excluded.* Note that by using a solar metallicity spectral library we are more likely to *underestimate*, rather than overestimate, M_{upp} in 30 Dor. Metal-poor O stars generally have weaker spectral features than those in the spectra of O stars in the solar vicinity, and a larger number of the most massive stars would be required to match the observations.

4.3. *The Stellar Number Counts*

We now compare the numbers of O and W-R stars predicted from the spectral synthesis models with those actually observed. Although we used values of N_{LyC} that were derived directly from Parker's (1992) star counts to normalize our models, we can nevertheless compare the numbers of O and W-R stars observed and computed in order to test the models.

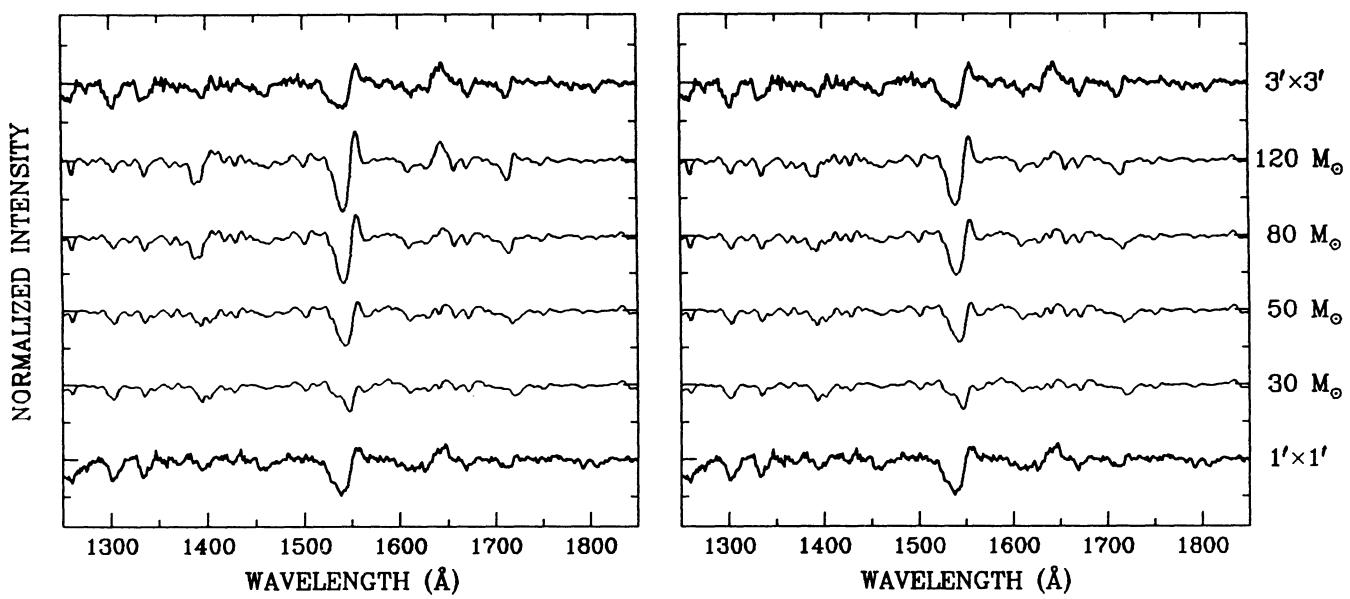

FIG. 7.—Observed (*thick lines at top and bottom*) and synthetic (*thin lines*) line spectra of 30 Dor. *Left:* Instantaneous burst; *right:* continuous burst. The effect of varying M_{upp} is shown. Model parameters are $Z = Z_\odot$, $\alpha = 2.35$, $M_{low} = 1\ M_\odot$, and $\tau = 2.5$ Myr.

From censuses given by Moffat et al. (1987), Campbell et al. (1992), and Parker (1992, 1993), we estimate that ~8–10 W-R stars are located within the 1′ × 1′ region and 13–17 W-R stars are located within the 3′ × 3′ region. (We excluded objects with "intermediate" spectral types, such as Of/WN, from the number of W-R stars.) Estimates of the number of O stars within these regions can be derived from Parker's ground-based data, supplemented with the recent results obtained by Malumuth & Heap (1994) using *HST* images of 30 Dor. Parker (1992, 1993) estimated effective temperatures for all the stars in his CCD frames, in addition to assigning spectral classifications to the bluest objects he identified. Using the criteria that all stars with either O-type spectral classifications or $T_{\rm eff} > 30{,}000$ K are O stars, we counted the number of stars within the two spatial regions of interest. Stars with spectral types intermediate between W-R and O (e.g., O3 If/WN6) were included as O stars; stars with spectral types listed as simply OB were excluded from the counts. From Parker's data, we estimate there are ~70 O stars within the 1′ × 1′ region and ~130 O stars in the 3′ × 3′ region.

As mentioned earlier (§ 3.2), Parker's ground-based images suffer from severe crowding in the immediate vicinity of R136, a problem which makes the photometry unreliable in this central region of the nebula. The fact that unresolved components are missed in Parker's stellar census implies that the estimated numbers of O stars within our 1′ × 1′ and 3′ × 3′ regions, as derived from his data, are actually lower limits. We attempted to obtain a more accurate estimate of the numbers of O stars in our regions by incorporating the results of Malumuth & Heap (1994). They used optical images acquired with *HST* to determine the massive stellar content in a 35″ × 35″ region centered on R136a. There are at least 184 stars in the images analyzed by Malumuth & Heap (1994) that are estimated to have masses larger than ~20 $M_\odot$. Since a temperature criterion for O stars of $T_{\rm eff} > 30{,}000$ K corresponds to a ZAMS mass of ~15 $M_\odot$ for the metallicity of the LMC (Vacca 1994), all of these objects could be O stars. (However, it should be emphasized again that few of the stars listed by Malumuth & Heap have definite spectral classifications and the number of O stars derived from their data is very uncertain and probably overestimated.) We then added this number to the number of O stars located *outside* the 35″ × 35″ region determined from Parker's data. With this procedure we estimated the number of O stars to be ~230 within the 1′ × 1′ region and 290 within the 3′ × 3′ region.

The number of O and W-R stars predicted from the spectral synthesis models for the two regions are given in Table 2 (for $Z = 0.25\ Z_\odot$) and Table 3 (for $Z = Z_\odot$) for a selected set of ages and upper cutoff masses. In the 1′ × 1′ region, the number of O stars predicted from the models varies between about 60 and 280 for an instantaneous burst, and between about 60 and 130 for a continuous burst, for ages $\tau \lesssim 5$ Myr, upper cutoff masses between $M_{\rm upp} = 60$ and 120 $M_\odot$, and a metallicity $Z = 0.25\ Z_\odot$. Similar ranges of values are found from $Z = Z_\odot$ models. The number of W-R stars may reach ~10 in the 1′ × 1′ region from an instantaneous burst at an age of $\tau = 5$ Myr and a metallicity of $0.25\ Z_\odot$, while smaller values (~2) are obtained from a continuous burst with the same parameters. For the 3′ × 3′ region, the instantaneous burst models with $Z = 0.25\ Z_\odot$ and $\tau \lesssim 5$ Myr yield between 120 and 560 O stars and up to 18 W-R stars. The continuous burst models, with the same parameters, yield at most three W-R stars and between about 120 and 260 O stars. Larger numbers of massive stars are required initially in the instantaneous burst scenario because these stars quickly evolve and contribute less to $N_{\rm LyC}$ with time. During a continuous burst, new stars are added at each time step and fewer very massive stars are required to produce the observed $N_{\rm LyC}$. Tables 2 and 3 also clearly demonstrate again the difficulty in distinguishing between the two burst scenarios when the burst is very young.

TABLE 2

PREDICTED HOT STAR POPULATIONS IN 30 DOR ($Z = 0.25\ Z_\odot$)

		1′ × 1′				3′ × 3′			
		Instantaneous Burst		Continuous Burst		Instantaneous Burst		Continuous Burst	
$M_{\rm upp}$ ($M_\odot$)	τ (Myr)	$N_{\rm W\text{-}R}$	$N_{\rm O}$	$N_{\rm W\text{-}R}$	$N_{\rm O}$	$N_{\rm W\text{-}R}$	$N_{\rm O}$	$N_{\rm W\text{-}R}$	$N_{\rm O}$
60	1.....	0	114	0	118	0	226	0	235
	2.....	0	113	0	116	0	226	0	232
	3.....	0	123	0	115	0	246	0	230
	4.....	0	208	0	123	0	416	0	245
	5.....	9	280	1	132	18	558	2	264
80	1.....	0	85	0	89	0	169	0	177
	2.....	0	84	0	87	0	168	0	174
	3.....	0	113	0	88	0	226	0	175
	4.....	6	130	1	94	13	260	1	188
	5.....	9	280	2	103	18	558	3	206
100	1.....	0	69	0	73	0	138	0	146
	2.....	0	69	0	71	0	139	0	142
	3.....	1	103	0	74	3	205	0	148
	4.....	6	131	1	79	13	261	2	158
	5.....	9	280	2	88	18	559	3	175
120	1.....	0	60	0	63	0	119	0	125
	2.....	0	62	0	61	0	124	0	123
	3.....	3	71	0	65	6	142	0	129
	4.....	7	131	1	70	13	260	2	139
	5.....	9	280	2	79	18	560	3	157

TABLE 3

PREDICTED HOT STAR POPULATIONS IN 30 DOR ($Z = Z_\odot$)

		1′ × 1′				3′ × 3′			
		Instantaneous Burst		Continuous Burst		Instantaneous Burst		Continuous Burst	
M_{upp} ($M_\odot$)	τ (Myr)	$N_{W\text{-}R}$	N_O	$N_{W\text{-}R}$	N_O	$N_{W\text{-}R}$	N_O	$N_{W\text{-}R}$	N_O
60	1.....	0	128	0	127	0	255	0	254
	2.....	0	120	0	123	0	240	0	246
	3.....	0	165	0	128	0	329	0	255
	4.....	29	214	2	140	58	428	3	279
	5.....	51	207	5	151	102	412	11	302
80	1.....	0	94	0	93	0	187	0	186
	2.....	0	91	0	92	0	181	0	184
	3.....	1	159	0	99	2	317	0	198
	4.....	35	207	3	106	71	414	6	211
	5.....	51	205	6	118	103	409	11	235
100	1.....	0	76	0	76	0	152	0	151
	2.....	0	78	0	76	0	155	0	152
	3.....	5	94	0	80	11	188	1	160
	4.....	36	208	3	87	72	415	6	173
	5.....	52	207	5	97	103	414	11	193
120	1.....	0	65	0	65	0	129	0	130
	2.....	0	68	0	65	0	135	0	130
	3.....	8	90	1	68	15	180	1	135
	4.....	36	208	3	76	71	415	7	151
	5.....	51	207	5	84	103	414	10	168

The entries in Table 2 indicate that the instantaneous burst model, with $\tau \lesssim 5$ Myr, $M_{upp} \gtrsim 60\ M_\odot$, and $Z = 0.25\ Z_\odot$, reproduces the observed numbers of W-R and O stars in both the 1′ × 1′ and the 3′ × 3′ regions reasonably well. For an age of ~3 Myr, as favored by the analysis of both the UV continua (see § 4.1) and the UV lines (see § 4.2), fewer W-R stars are predicted by the model than are observed in the regions, unless the upper cutoff mass is very large ($M_{upp} \sim 120\ M_\odot$). However, it should be remembered that both the number of O stars observed in 30 Dor and the number of W-R stars predicted from the evolutionary models are rather uncertain. For example, changing the values of N_{LyC} used to normalize the models by a factor of 2 changes the predicted numbers of W-R and O stars in the regions by a factor of 2. In addition, the onset of the W-R phase in Maeder's (1990) evolutionary tracks is highly dependent on the adopted mass-loss rates and their variation with metallicity, both of which have large uncertainties (e.g., Maeder & Meynet 1994). Nevertheless, the relatively large number of W-R stars in the center of 30 Dor seems to favor an instantaneous burst scenario. If the burst is continuous, then it can have a duration of at most only a few million years.

5. DISCUSSION

From the combined results of our spectral synthesis analysis of the observed UV continuum spectra and the observed UV line spectra, and a comparison of the numbers of O and W-R stars actually observed with those predicted by the models, we conclude that, in the central 1′ × 1′ and 3′ × 3′ regions of 30 Dor, the age of the starburst episode has an *upper limit* of $\tau \lesssim 3$ Myr and the present-day value of the upper cutoff mass of the IMF has a *lower limit* of $M_{upp} \gtrsim 50\ M_\odot$. Low values of M_{upp} (e.g., $M_{upp} \lesssim 40\ M_\odot$) are inconsistent with the observed UV line profiles and continua. An example of a good fit of a synthesized spectrum to the spectrum observed from the 1′ × 1′ region is shown in Figure 8. The parameters for the instantaneous burst model shown are $\tau = 3.15$ Myr, $M_{upp} = 60\ M_\odot$, and $Z = 0.25 Z_\odot$. All of our models assume that the slope of the IMF is $\alpha = 2.35$. We place particular emphasis on the results from the synthesis analysis of the line spectra, as these are unaffected by uncertainties in the color excess, extinction law, or the number of stars identified in the crowded fields in and near the core of 30 Dor. Although the quantities derived from the analysis of the UV continua are highly dependent on the color excess and the extinction law used to deredden the spectra, the extinction toward 30 Dor is fairly well understood. We should also emphasize that the values of N_{LyC} used to normalize our models, and derived from Parker's (1992) estimates of the stellar population, are most likely lower limits. Values of N_{LyC} larger than that used here only strengthen our conclusions regarding the age and upper cutoff mass limits in 30 Dor.

The lower limit to the upper cutoff mass inferred from our spectral synthesis analysis agrees nicely with the results of Parker (1992) and Parker & Garmany (1993), who constructed an IMF for the region using ground-based photometry and spectroscopy of stars within the region. They found that the most massive objects in the region had initial masses $M \gtrsim 85\ M_\odot$. Our results also agree with those presented by Heap et al. (1992) and Malumuth & Heap (1994), who analyzed images obtained with *HST* and estimated that the most massive O stars in the region had initial masses of $\sim 70\ M_\odot$. Neither of these estimates take account of the initial masses of the O stars that presumably have evolved to become the W-R stars currently observed in the regions.

The upper limit of ~3 Myr to the age of the starburst in the regions we observed with *IUE* also agrees extremely well with other determinations (Walborn 1991a, b; Heap et al. 1992; De Marchi et al. 1993; Meylan 1993; Malumuth & Heap 1994). Although we did not fully investigate this scenario, the results of the spectral synthesis analysis may suggest the occurrence of multiple bursts within the 3′ × 3′ region, a possibility which is

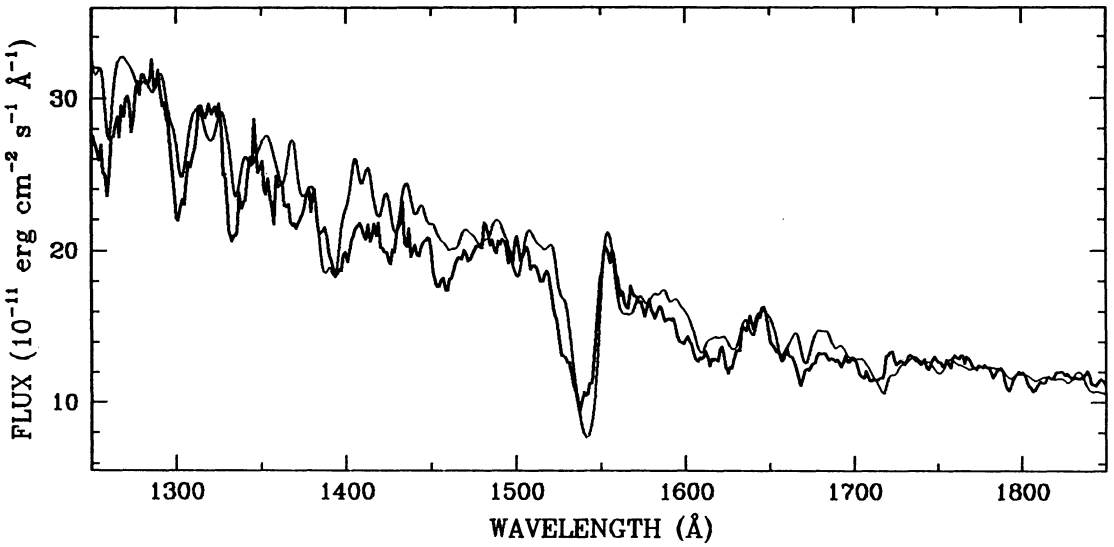

FIG. 8.—Observed spectrum (*thick line*) and best-fitting synthetic spectrum from an instantaneous burst model (*thin line*) for the central 1′ × 1′ region of 30 Dor. Model parameters are $Z = 0.25\ Z_{\odot}$, $\alpha = 2.35$, $M_{low} = 1\ M_{\odot}$, $M_{upp} = 60\ M_{\odot}$, and $\tau = 3.15$ Myr.

in accord with the spread in the inferred ages of stars in the region (Walborn 1986). Age gradients and sequential star formation scenarios in 30 Dor have been previously discussed by many workers (e.g., Hyland, Thomas, & Robinson 1978; McGregor & Hyland 1981; Walborn 1986; Hyland & Jones 1991; Lortet & Testor 1991; Walborn & Parker 1992; Parker & Garmany 1993). The difficulty in reproducing the observed spectrum for the 3′ × 3′ region might also be due to mass segregation and spatial variations in the IMF (e.g., Malumuth & Heap 1994). These phenomena may themselves be direct results of multiple star formation episodes within the region.

The numbers of O stars predicted from our spectral synthesis models agree with several estimates of the hot star populations in the regions, as determined from both ground-based (Parker 1992; Parker & Garmany 1993) and *HST* (Campbell et al. 1992; De Marchi et al. 1993; Malumuth & Heap 1994) data. Similarly, the predicted numbers of W-R stars in the regions are consistent with other determinations and censuses (Moffat et al. 1987; Campbell et al. 1992). Our models were normalized to produce the number of Lyman continuum photons estimated from Parker's (1992) determination of the stellar content within the regions, so these results were somewhat expected. However, the agreement serves to increase our confidence in the spectral synthesis models.

Finally, there remain a few additional points regarding both the observed spectra and the spectral synthesis analysis that are worth noting. The dereddened UV continuum spectra of the 1′ × 1′ and 3′ × 3′ regions exhibit a nearly power-law shape, $F_{\lambda} \sim \lambda^{-\beta}$, with a slope of $\beta \approx 2.5$. Although this value of the slope is consistent with that observed for the intrinsic spectra of hot stars (O and W-R stars), it is significantly larger than the averages found by Kinney et al. (1993) for starburst galaxies ($\beta = 1.25$) and blue compact/H II galaxies ($\beta = 1.75$). This is somewhat surprising, as the UV spectra of these galaxies are thought to be dominated by emission from regions similar to 30 Dor. However, Kinney et al. (1993) assumed that the shape of the extinction laws within the galaxies they studied was similar to that of our Galaxy. In fact, the extinction laws within these galaxies may be substantially different from that of either our own Galaxy or the LMC (e.g., Calzetti, Kinney, & Storchi-Bergmann 1994; Kinney et al. 1994; Rosa & Benvenuti 1994). The differences in the intrinsic continuum slopes between 30 Dor and those of the starburst and blue compact/H II galaxies may be due solely to differences in the shapes of the extinction laws (Kinney et al. 1994). The advantage of studying 30 Dor is that the internal reddening law, as well as the internal and Galactic foreground color excesses, are known rather accurately.

Figures 2*a* and 2*b* reveal striking differences in the strength of the C III] λ1909 emission line in the spectra of the three regions observed with *IUE*. The spectrum of the 3′ × 3′ region exhibits a particularly strong and broad emission line, and here we consider three possibilities for producing this feature: the fast winds of W-R stars, shock excitation of nebular gas, and photoionization of nebular gas. The C III] λ1909 line is a prominent emission line in the UV spectra of early WC (WCE) stars. Moffat et al. (1987) estimated there are about three WCE stars located within 1′.5 of R136a. Although the very broad profile of the C III] λ1909 line seen in our spectra seems to suggest that this line is produced primarily in high-velocity stellar winds, comparison of the flux observed for the line in the spectrum of the 3′ × 3′ region with an average flux value for this line derived from the spectra of individual WCE stars (K. R. Brownsberger 1994, private communication) indicates that three WCE stars can account for at most 10%–20% of the observed emission strength. Shock excitation of the C III] λ1909 line can also be ruled out. There is no evidence for other emission lines (e.g., O III] λ1663; Shull & Draine 1987) which would be expected to be present in the spectrum at a strength comparable to that of C III] λ1909 if this line were produced primarily by shocks with expansion velocities $\lesssim 200$ km s^{-1} (Chu & Kennicutt 1994). Therefore, we are left with photoionization as the source of the C III] λ1909 line. The differences in the strengths of this line in the various spectra must be due simply to the different geometrical surface areas (and therefore different volumes of line-emitting gas) for the regions observed.

From the value of N_{LyC} used for our analysis of the spectrum of the 3′ × 3′ region, we can predict the flux in the correspond-

ing Hβ emission line, and thereby derive an estimate of the C III] λ1909/Hβ intensity ratio. We find this ratio to be $\sim$0.1, a value which is consistent with that predicted by photoionization models of H II regions with $T_{\rm eff} \approx$ 35,000 K and $Z = 0.2\ Z_{\odot}$ (Stasińska 1990). This result, in addition to the fact that the observed line fluxes in the various spectra scale roughly with the areas of the regions, confirms the idea that the observed emission line is produced primarily by photoionization. Substantial nebular emission from photoionized gas within the $3' \times 3'$ region might also provide a partial explanation for the relatively poor fit between the synthesized and observed C IV λ1550 line profiles. Although the models of Stasińska (1990) indicate that nebular C IV λ1550 emission is very weak if $T_{\rm eff} =$ 35,000 K, small regions of gas near a few of the very hottest stars might contribute significantly to the observed integrated C IV λ1550 line profile. In this case, our models, which use purely stellar spectra to synthesize line profiles, would be unable to accurately reproduce the observed line shape.

6. CONCLUSIONS

The possibility of comparing the global properties of a giant extragalactic H II region with the known stellar population in the region makes the study of 30 Dor particularly important and useful to the understanding of more distant unresolved starburst regions. With the spatially integrated UV spectra obtained with *IUE*, we can treat 30 Dor as though it were a distant unresolved starburst region and then compare the results of our spectral analysis with the known properties, as derived from detailed studies of the individual components. With these spectra we have at our disposal both the dereddened UV continua and the observed UV line strengths and profiles as *independent* constraints on the parameters of the hot star populations and the starburst episodes. The UV lines and continua are sensitive to, and provide limits on, the age and duration of the starburst episode, the upper cutoff mass of the IMF in the region, and the total number of stars present. Any model which successfully reproduces the continua and line features of the observed spectra must then also predict the correct (i.e., observed) numbers of O and W-R stars in the 30 Dor region.

We have used the spectral synthesis models of Leitherer et al. (1992b) and Robert et al. (1993) to analyze the spatially integrated UV spectra of two regions centered on R136 in 30 Dor. We find that models incorporating an instantaneous burst of star formation with an age of less than $\sim$3 Myr, and an upper cutoff mass of the IMF of $\gtrsim$50 $M_{\odot}$, can adequately reproduce both the observed UV continuum flux levels and the observed UV line profiles. Our results agree very well with other estimates of the age and upper cutoff mass in the regions. The total numbers of O and W-R stars predicted from the models also agree reasonably well with the actual star counts in the area, as determined from both ground-based and *HST* observations. Although the predicted number counts seem to favor an instantaneous burst over a continuous burst, the very young age of the starburst episode in the central regions of 30 Dor makes the task of distinguishing between the two burst scenarios difficult. We conclude that the spectral synthesis models of Leitherer et al. (1992b) and Robert et al. (1993) can be used to determine the observed hot star populations in a complex star-forming region fairly accurately. We can now proceed with confidence to perform UV spectral synthesis analyses of more distant extragalactic H II regions and starbursts for which we have *IUE* and *HST* spectrophotometry.

The authors are extremely grateful to Joel Parker for producing and providing them with Figure 1. He also supplied several important numbers and tables derived from his study of the stellar populations in 30 Dor and graciously answered numerous questions about both his own work on the region and that of others. We are also deeply indebted to Rob Kennicutt for reanalyzing his Hα images of 30 Dor and providing us with fluxes within specified regions. We would also like to acknowledge useful discussions with Mark Phillips and Matt Garhart regarding the reduction of *IUE* data. We thank the referee, Eliot Malumuth, for a detailed report and numerous comments which helped to improve the manuscript. W. D. V. is supported by NASA through grant HF-102.01-91A, awarded by the Space Telescope Science Institute, which is operated by the Association of Universities for Research in Astronomy, Inc., for NASA under contract NAS 5-26555. C. R. thanks NSERC (Canada) for a postdoctoral fellowship and STScI's Director's Research Fund (WBS 82014) for travel support. P. S. C. acknowledges support for this work from NASA under (*IUE*) grant NAG 5-1016. The *IUE* RDAF at the University of Colorado, where some of the data reduction for this project was performed, was supported by NASA grant NAS 5-28731. Additional support for this work was provided by NASA through grant GO-3591.01-91A from the Space Telescope Science Institute.

REFERENCES

Bessell, M. S. 1991, A&A, 242, L17
Blades, J. C. Wheatley, J. M., Panagia, N., Grewing, M., Pettini, M., & Wamsteker, W. 1988, ApJ, 334, 308
Calzetti, D., Kinney, A. L., & Storchi-Bergmann, T. 1994, ApJ, 429, 582
Campbell, B., et al. 1992, AJ, 104, 1721
Conti, P. S., Leep, E. M., & Perry, D. N. 1983, ApJ, 268, 228
Chu, Y.-H., & Kennicutt, R. C. 1994, ApJ, 425, 720
De Marchi, G., Nota, A., Leitherer, C., Ragazzoni, R., & Barbieri, C. 1993, ApJ, 419, 658
Dufour, R. J. 1984, in IAU Symp. 108, The Structure of the Magellanic Clouds, ed. S. Van den Bergh & K. S. de Boer (Dordrecht: Reidel), 353
Esteban, C., Smith, L. J., Vilchez, J. M., & Clegg, R. E. S. 1993, A&A, 272, 299
Fitzpatrick, E. L. 1986, AJ, 92, 1068
Fitzpatrick, E. L., & Savage, B. D. 1984, ApJ, 279, 578
Garhart, M. P. 1992a, NASA IUE Newsletter, 48, 88
———. 1992b, NASA IUE Newsletter, 48, 98
Garmany, C. D., & Conti, P. S. 1985, ApJ, 293, 407
Heap, S. R., Ebbets, D., & Malumuth, E. M. 1992, in Science with the Hubble Telescope, ed. P. Benvenuti & E. Schreier (Garching: ESO), 347
Hill, J. K., et al. 1993, ApJ, 413, 604
Horne, K. 1986, PASP, 98, 609
Hyland, A. R., & Jones, T. J. 1991, in IAU Symp. 148, The Magellanic Clouds, ed. R. Haynes & D. Milne (Dordrecht: Kluwer), 202
Hyland, A. R., Thomas, A. J., & Robinson, G. 1978, AJ, 83, 20
Israel, F. P., & Koornneef, J. 1979, ApJ, 230, 390
Kennicutt, R. C., Jr., & Chu, Y.-H. 1994, in Violent Star Formation, from 30 Doradus to QSOs, ed. G. Tenorio-Tagle (Cambridge: Cambridge Univ. Press), 1
Kennicutt, R. C., Jr., & Hodge, P. W. 1986, ApJ, 306, 130
Kinney, A. L., Bohlin, R. C., Calzetti, D., Panagia, N., & Wyse, R. F. G. 1993, ApJS, 86, 5
Kinney, A. L., Bohlin, R. C., & Neill, J. D. 1991, PASP, 103, 694
Kinney, A. L., Calzetti, D., Bica, E., & Storchi-Bergmann, T. 1994, ApJ, 429, 172
Kurucz, R. L. 1992, in IAU Symp 149, The Stellar Population of Galaxies, ed. B. Barbuy & A. Renzini (Dordrecht: Kluwer), 225
Lee, M. G. 1990, PhD. thesis, Univ. Washington
Leitherer, C., Gruenwald, R., & Schmutz, W. 1992a, in Physics of Nearby Galaxies, ed. T. X. Thuan, C. Balkowski, & J. T. T. Van (Gif-sur-Yvette: Editions Frontières), 257
Leitherer, C., & Heckman, T. M. 1995, ApJS, 96, 9
Leitherer, C., & Lamers, H. J. G. L. M. 1991, ApJ, 373, 89
Leitherer, C., Robert, C., & Drissen, L. 1992b, ApJ, 401, 596
Lortet, M.-C., & Testor, G. 1991, A&AS, 89, 185
Maeder, A. 1990, A&AS, 84, 139
Maeder, A., & Meynet, G. 1988, A&AS, 76, 411

Maeder, A., & Meynet, G. 1994, A&A, 287, 803
Malumuth, E. M., & Heap, S. R. 1994, AJ, 107, 1054
Mathis, J. S., Chu, Y.-H., & Peterson, D. E. 1985, ApJ, 292, 155
McGregor, P. J., & Hyland, A. R. 1981, ApJ, 250, 116
McNamara, D. H., & Feltz, K. A. 1980, PASP, 92, 587
Melnick, J. 1985, A&A, 153, 235
Meylan, G. 1993, in The Globular Cluster-Galaxy Connection, ed. G. H. Smith & J. P. Brodie (San Francisco: ASP), 588
Mills, B. Y., Turtle, A. J., & Watkinson, A. 1978, MNRAS, 185, 263
Moffat, A. F. J., Niemela, V. S., Phillips, M. M., Chu, Y.-H., & Seggewiss, W. 1987, ApJ, 312. 612
Morris, P. W., Brownsberger, K. R., Conti, P. S., Massey, P., & Vacca, W. D. 1993, ApJ, 412, 324
Panagia, N., Gilmozzi, R., Macchetto, F., Adorf, H. M., & Kirshner, R. P. 1991, ApJ, 380, L23
Parker, J. W. 1992, Ph.D. thesis, Univ. Colorado
———. 1993, AJ, 106, 560
Parker, J. W., & Garmany, C. D. 1993, AJ, 106, 1471
Robert, C., Leitherer, C., & Heckman, T. M. 1993, ApJ, 418, 749
Rosa, M., & Mathis, J. S. 1987, ApJ, 317, 163
Rosa, M. R., & Benvenuti, P. 1994, A&A, 291, 1
Salpeter, E. E. 1955, ApJ, 121, 161
Schmidt-Kaler, T. 1982, in Landolt-Börnstein IV: Numerical Data and Functional Relationships in Science and Technology, Vol. 2b, ed. K. Schaifers & H. H. Voigt (Berlin: Springer), 1
Schmutz, W., Leitherer, C., & Gruenwald, R. 1992, PASP, 104, 1164
Seaton, M. J. 1979, MNRAS, 187, 73
Shull, J. M., & Draine, B. T. 1987, in Interstellar Processes, ed. D. J. Hollenbach & H. A. Thronson, Jr. (Dordrecht: Reidel), 283
Smith, L. F., & Hummer, D. G. 1988, MNRAS, 230, 511
Smith, L. F., & Maeder, A. 1991, A&A, 241, 77
Stasińska, G. 1990, A&AS, 83, 501
Vacca, W. D. 1991, Ph.D. thesis, Univ. Colorado
———. 1994, ApJ, 421, 140
Vacca, W. D., Conti, P. S., & Phillips, M. 1995, in preparation
Walborn, N. R. 1984, in IAU Symp. 108, Structure and Evolution of the Magellanic Clouds, ed. S. van den Bergh & K. S. de Boer (Dordrecht: Reidel), 243
———. 1986, in IAU Symp. 116, Luminous Stars and Associations in Galaxies, ed. C. W. H. de Loore, A. J. Willis, & P. Laskarides (Dordrecht: Reidel), 185
———. 1991a, in IAU Symp. 148, The Magellanic Clouds, ed. R. Haynes & D. Milne (Dordrecht: Kluwer), 145
———. 1991b, in Massive Stars in Starbursts, ed. C. Leitherer, N. Walborn, T. Heckman, & C. Norman (Cambridge: Cambridge Univ. Press), 145
Walborn, N. R., & Panek, R. J. 1984a, ApJ, 280, L27
———. 1984b, ApJ, 286, 718
Walborn, N. R., & Parker, J. W. 1992, ApJ, 399, L87
Weigelt, G., et al. 1991, ApJ, 378, L21